JOC The Journal of Organic Chemistry

pubs.acs.org/joc Article

Ultrafast Photoelimination of Nitrogen from Upper Excited States of Diazoalkanes and the Fate of Carbenes Formed in the Reaction

Vedran Brusar, Mateo Forjan, Ivan Ljubić,* Marija Alešković, Kristin Becker, and Silvije Vdović*

Cite This: J. Org. Chem. 2023, 88, 4286−4300 Read Online

ACCESS | Metrics & More | Article Recommendations | Supporting Information

ABSTRACT: The photochemical reactivity of diphenyldiazomethane **1** and phenyl 1- and 2-adamantyl diazomethanes **2** and **3**, respectively, was investigated by transient absorption spectroscopy (TA). Photoelimination of N_2 upon UV excitation takes place in the anti-Kasha ultrafast photochemical reaction from the upper excited singlet states to deliver singlet carbenes, which were, in the case of **1** and **2**, detected by fs-TA. The reactivity of the carbenes differs with respect to the substituent at the carbene center. The singlet **car-1** in a nonpolar solvent delivers the triplet carbene by intersystem crossing (ISC). Singlet **car-2** does not undergo ISC but reacts in the intermolecular insertion reactions into C−H bonds. **Car-3** has an α-C−H bond next to the carbene center and reacts rapidly in the intramolecular C−H insertion reaction to deliver alkene, precluding its detection by fs-TA. However, the isolation of ketone photoproducts from **3** is highly indicative of triplet **car-3**'s intermediate formation. The TA spectra from the S_1−S_3 states of **1**−**3** were computed using time-dependent density functional theory, while the multiconfigurational perturbation theory to the second order was used for the absorption spectra of the corresponding singlet and triplet carbenes. The modeled and measured spectra are in good agreement, and the computations corroborate the assignments of the key short-lived intermediates.

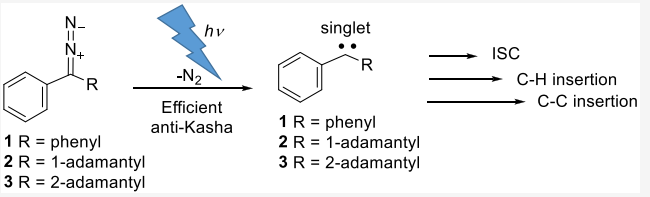

INTRODUCTION

Since the seminal papers of Hine[1] and van Doering,[2] carbene chemistry has developed into intensively investigated topic,[3−5] primarily due to the applications of stable carbenes[6] in catalysis.[7,8] Moreover, significant endeavors were undertaken in the investigation of physical−organic aspects of carbene chemistry[9] and to elucidate carbene reaction mechanisms and reactivity.[10] One important reaction to generate carbenes is thermally or photochemically induced elimination of nitrogen from diazoalkanes,[11] which can also be used in biological systems.[12,13] Diazoalkanes are versatile reagents in organic synthesis.[14] Thus, diazomethane has been known for more than a century and is used in the methylation of carboxylic acids, alcohols, and phenols; cyclopropanations; ring expansions; and cycloadditions.[15] Moreover, the use of diazo compounds has been demonstrated in stereoselective synthesis[16] or in combination with transition metals and catalysis.[17,18]

The photochemical reaction mechanism for the elimination of nitrogen from diazoalkanes has been investigated by several groups.[19−21] Moreover, Piteša et al. recently showed that the elimination of nitrogen takes place more efficiently upon excitation to higher singlet excited states in the anti-Kasha photochemical reactions.[22] Anti-Kasha photochemical reactivity has also been demonstrated in the photoelimination of nitrogen from Meldrum's acid, whereupon ketenes are formed in the Wolff rearrangement,[23] while subsequent ultrafast studies on this system explored the dynamics of carbene formation from S_2.[24] However, for diverse molecules, some questions still remain open, such as if carbene intermediates are formed in the photoelimination of nitrogen from diazo compounds having an α-H atom with respect to the diazo group or if N_2 elimination and α-C−H insertion take place simultaneously[4] in the rearrangements in the excited state (RIES).[25−29] The RIES has been debated for the elimination of carbenes from diazirines,[30] as well as for diazo compounds.[19,31]

Here we report on the investigation of carbene formation from diazo carbene precursors **1**−**3** (Figure 1) by femtosecond transient absorption spectroscopy (fs-TA) and laser flash photolysis (LFP). The findings were corroborated by the computations of the transient spectra carried out in the framework of time-dependent density functional theory and multiconfigurational perturbation theory to the second order. Our experiments provide the first direct experimental spectroscopic evidence for carbene generation directly from the FC state in the anti-Kasha photochemical reaction. The anti-Kasha photochemistry is gaining importance, as it provides new opportunities for fine-tuning the reactivity by the appropriate choice of light wavelength.[32] Moreover, we present

Received: November 30, 2022
Published: March 21, 2023

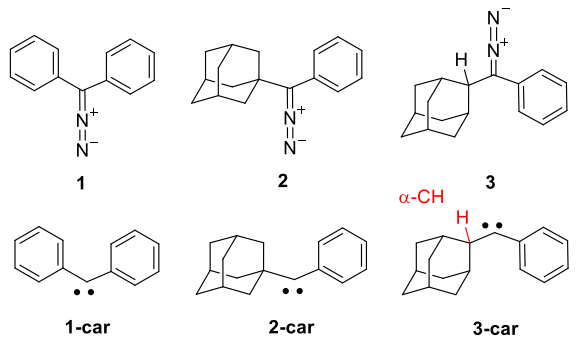

Figure 1. Investigated diazo derivatives **1**−**3** and the corresponding carbenes **car-1**−**3**.

evidence for carbene generation from both adamantyl precursors **2** and **3**, although the latter has an α-C−H bond to the carbene center.

RESULTS AND DISCUSSION

Photochemical generation of carbenes from **1** and the chemistry of the corresponding carbenes has been intensively investigated.[33−44] Furthermore, the synthesis and photochemistry of **2** have been reported by Eguchi et al.[45] and Piteša et al.,[22] whereas **3** has hitherto never been prepared. The details on the syntheses of **1**−**3** are given in the Experimental and Computational Details and in the Supporting Information (Schemes S1−S3 in the SI).

Ground-State Structures, Conformations, and Relative Energies. Figure 2 depicts the structures of the ground states and S_1 and T_1 minima of **1**, **2**, and **3** with the indicated relevant geometric parameters. The corresponding Cartesian coordinates and harmonic frequencies are given in Table S7 in the SI. Using the CAM-B3LYP(+PCM)/6-311+G(2d,p) level, the global conformational minima of **1**, **2**, and **3** and their corresponding carbenes were found by performing the relaxed structural scans with respect to the torsion around the C−C(N_2) bonds. The energy difference between the minimum and maximum rotamer in **3** is found to be 6.3 kcal mol^{-1} in contrast to the nearly free rotation in **1** and **2**, where these differences are only 1.6 and 1.4 kcal mol^{-1}. The minimum conformers of **1** and singlet and triplet **car-1** exhibit the C_2 point group symmetry; similar structures were reported previously.[22,40] The conformational preferences in **1**, **2**, and **3** reflect the compromise between the reduction of the steric strain with respect to the two bulky substituents and the enhancement of the conjugation between the C−N−N and benzene π-densities. The two opposing effects determine the optimal angles closed by the C−N−N axis and the plane of the benzene ring, which equal 29°, 7°, and 19° in **1**, **2**, and **3**,

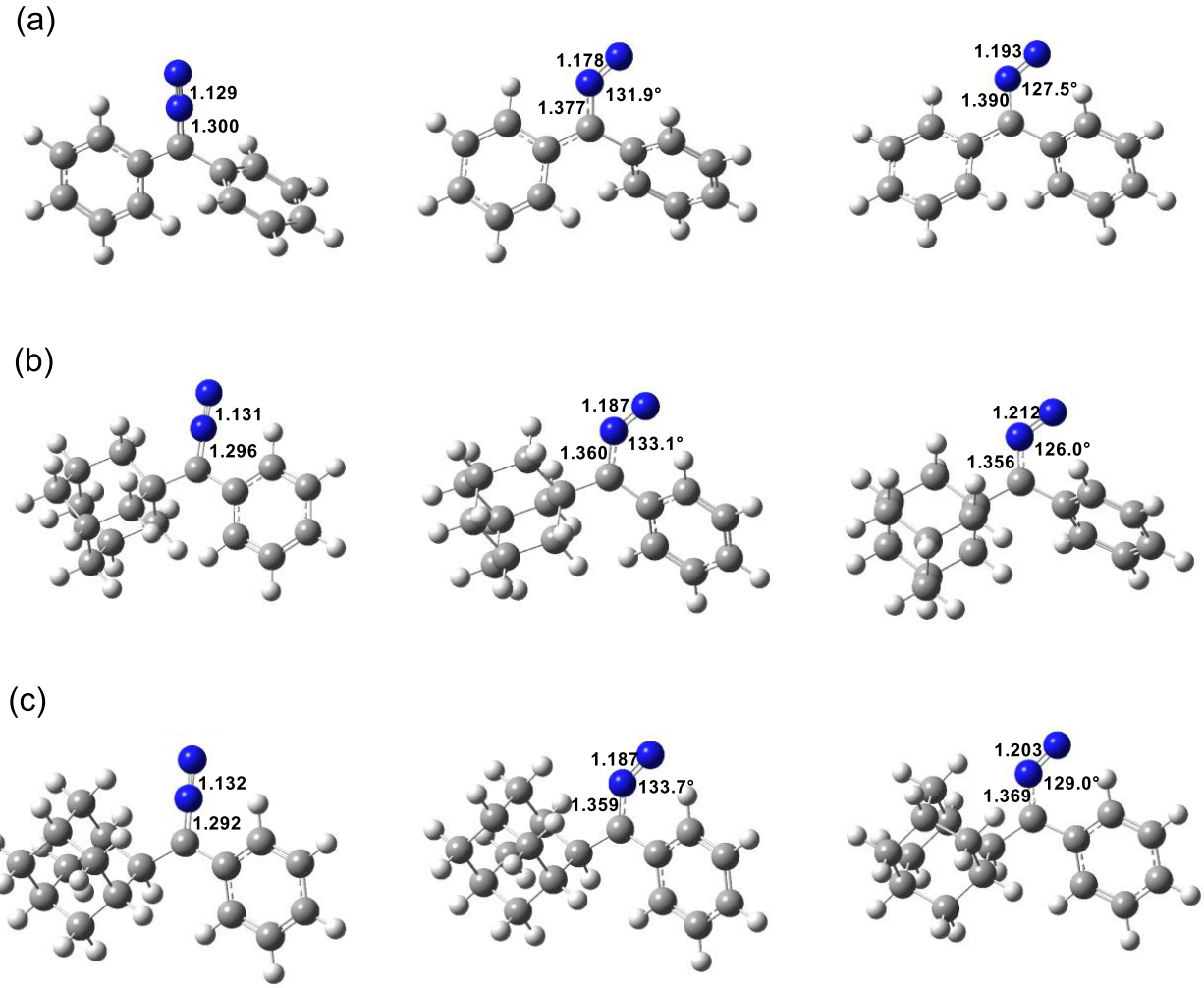

Figure 2. C−N and N−N bond lengths (Å) and C−N−N angles in the minimum geometries of the S_0, S_1, and T_1 states of (a) **1**, (b) **2**, and (c) **3**.

https://doi.org/10.1021/acs.joc.2c02875
J. Org. Chem. 2023, 88, 4286−4300

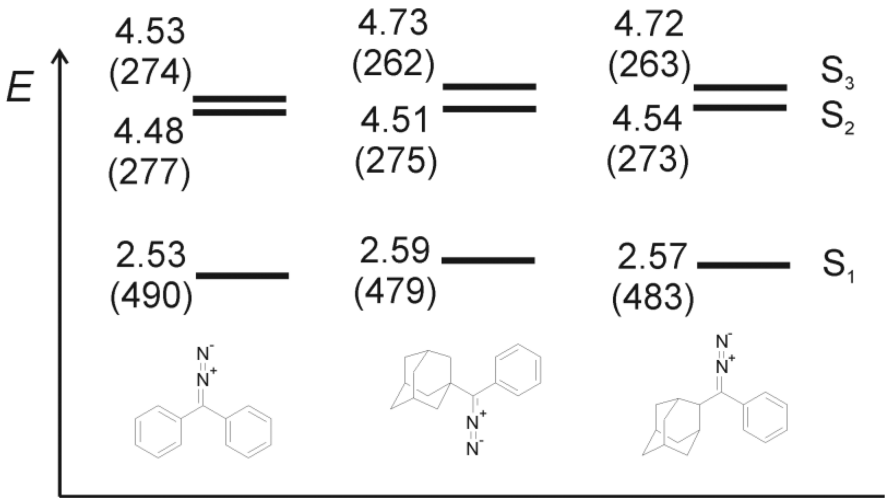

Figure 3. Energy diagram (the levels are given in eV (nm)) corresponding to the first three singlet excited states (S_1, S_2, and S_3) of **1**, **2**, and **3** computed at the TD-CAM-B3LYP(+PCM)/6-311+G(2d,p) level.

respectively. The vertical first ionization potentials (IP) computed at the EPT-P3+/cc-pVTZ level equal 7.416, 7.364, and 7.421 eV for **1**, **2**, and **3**, respectively. They mirror the stabilities of the corresponding HOMOs depicted in Figure S15 in the SI.

Another factor that influences the conformational minima of **2** and **3** is the hyperconjugation. Here this effect concerns the stabilizing interaction of C−N−N and the benzene ring π-density with the adjacent σ(C−H) and σ(C−C) bonds of the adamantyl moiety. The HOMOs of **2** and **3** (Figure S15) clearly show how the π-density is delocalized over these σ-bonds. By applying energy decomposition analysis, it has been shown that a σ(C−H) bond in interactions with various π-systems typically gives rise to larger orbital stabilization terms than a σ(C−C) bond.[46] This is also the case here and leads to the larger first IP and the more hindered rotation in **3** compared to **2** (vide supra). Likewise, the wavenumbers for the corresponding torsional motion are 12 and 27 cm^{-1} in **2** and **3**, respectively (Table S7 in the SI).

The triplet carbenes are in all cases predicted to be more stable than their singlet counterparts. The CAM-B3LYP-(+PCM) method gives the singlet−triplet (S-T) free-energy gaps (298 K) of 7.4, 9.4, and 7.3 kcal mol^{-1} for **car-1**, **car-2**, and **car-3**, respectively. The tangibly greater stabilization of triplet **car-2** compared to the **car-1** and **car-3** triplets is also confirmed by the CASPT2 method (0 K; ZPE not included); the gaps here are 5.3, 11.1, and 7.3 kcal mol^{-1}, respectively.

Photophysical Properties. Prior to conducting photochemistry, we investigated the photophysical properties of **3**, whereas the photophysical properties of **1** and **2** have been disclosed.[22,32−43] Absorption and fluorescence spectra of **3** were recorded in pentane and benzene (see Figures S1−S3 in the SI). They show the same features reported for **2**.[21] The diazo compounds are characterized by two absorption bands. The band at ≈500 nm is very weak, whereas that at ≈300 nm is very strong. The two can be correlated with the transitions to the S_1−S_3 excited states, which in the TD-CAM-B3LYP spectra of **2** (**3**) are found at 479 (483), 275 (273), and 262 (263) nm carrying the respective oscillator strengths of 0.000 (0.001), 0.414 (0.409), and 0.090 (0.101). The energies of the first three vertical transitions are diagrammed in Figure 3. The full computed absorption spectra are provided in Table S4 in the SI. In the natural transition orbital (NTO) picture, the relative strength of these transitions can be rationalized by the local symmetry properties of the initial and final π-orbitals. Thus, the transition to S_1 is weak because the involved π-orbitals are mutually orthogonal (analogous to the $n \rightarrow \pi^*$ transition; Figure S16 in the SI) while the transition to S_2 is strong because the π-orbitals are parallel (analogous to the $\pi \rightarrow \pi^*$ transition; Figure S17 in the SI). The relatively large energy gap of more than 2 eV between S_1 and S_2 for this class of compounds is in agreement with the previous results[22] and is here also confirmed for **3**. In modeling the early TA spectra corresponding to the vertical (FC) geometries (vide infra), we consider the contributions of both S_2 and S_3, as in **1**, **2**, and **3** these states are separated by only 0.1 eV and the transition to S_3 is still sufficiently intense (Table S4 in the SI).

Similar to **2**, but unlike **1**, **3** is weakly fluorescent when excited to S_n, with a quantum yield of fluorescence $\Phi_F \approx 0.04$. Upon excitation to S_1, fluorescence could not be detected (Figure S3 in the SI). The results indicate that fluorescence takes place from S_n prior to internal conversion (IC) to S_1. The finding can be explained by a large energy gap between S_1 and S_n, which results in weak nonadiabatic coupling between these states and slow IC transitions. The decay of fluorescence for **2** and **3** in benzene was fit to a biexponential function, suggesting more complex photophysics involving at least two excited states (Table S3 in the SI). Note, however, that nanosecond fluorescence lifetimes are in contradiction with the observed anti-Kasha photochemical reactivity from higher excited states that takes place in subpicosecond time scale (vide infra). This inconsistency may be explained by different excited states involved in photoreaction or emission.

Photochemistry. Prompted by the observation of fluorescence for **2** and **3**, we investigated if these molecules show anti-Kasha photochemistry. Preparative irradiations for **2**[22] and **3** were performed in cyclohexane and benzene upon excitation with visible light (cool white lamps, corresponding to the population of S_1) or at ≈300 nm, giving rise to a population of S_n (where $n > 1$).

Upon the irradiation of **3** in cyclohexane, **15** was formed as the major product, resulting from carbene insertion into the α-C−H bond (Scheme 1 and Table S1 in the SI). Isolation of the photoproducts was performed by TLC or column chromatog-

https://doi.org/10.1021/acs.joc.2c02875
J. Org. Chem. 2023, 88, 4286−4300

Scheme 1. Photolysis of 3

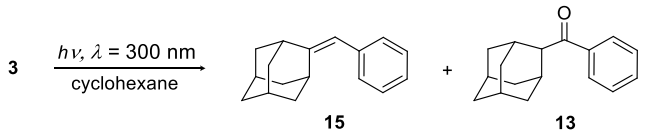

raphy. In addition, we isolated some smaller amounts of ketone **13** that formed due to the traces of dissolved oxygen in the solvent, which is a strong indication that the carbene intermediate was present in the solution. It is generally known that singlet carbenes react with O_2 slowly ($k < 10^7$ M^{-1} s^{-1}), whereas the reaction of triplet carbenes with O_2 is much faster ($k = 10^8-10^{10}$ M^{-1} s^{-1}).[5] Therefore, products from the irradiation of **3** in cyclohexane indicate the formation of both singlet and triplet carbene intermediates, as reported in the photochemistry of adamantane diazirine.[47] The quantum yield for the elimination of nitrogen (Φ_R) upon excitation at 300 nm or by visible light was measured using a ferrioxalate actinometer (for details, see Table S2) in the SI.[48,49] In agreement with the photochemistry of **1** and **2**,[22] Φ_R is almost an order of magnitude larger upon excitation to a higher singlet excited state at 300 nm ($\Phi_R = 0.34-0.36$) than upon excitation to S_1 ($\Phi_R = 0.005-0.1$), indicating that **3** also undergoes anti-Kasha photochemistry.

Excited States and Transient Species. The strongest transitions in the excited-state absorption (ESA) spectra of **1**, **2**, and **3** computed at the S_0 (FC) minimum geometries are shown in Table 1. Additional strong transitions, e.g., for the transient spectra calculated at the S_1 minimum geometries, are provided in Table S5. The ESA spectra modeled using the Gaussian broadening with the full-width-at-half-maximum parameter set to 3000 cm^{-1} are shown below (Figures 4, 6, and 8). The NTOs for the strongest ESA transitions in the FC S_1 spectra computed at the TD-CAM-B3LYP(+PCM)/ma-def2-TZVP(-f) level are depicted in Figure S16 in the SI. Some of the excited states, which give rise to weak transitions from the S_0 ground state, can become very bright when the transition originates from S_{1-3}. It is invariably found that in the case of the strongest transitions, the two involved excited states have closely similar dominant particle NTOs, as is observed, for example, for the $S_1 \rightarrow S_{12}$ transition in **1** (Figure S16).

Table 1. Strongest Transitions in the Transient Spectra of 1, 2, and 3 for the Relevant Spectral Region Computed at the S_0 (FC) Minimum Geometries Using the TD-CAM-B3LYP(+CPCM)/ma-def2-TZVP(-f) Level

	$I \rightarrow F$[a]	f[b]	E (eV) (nm)
1	1 → 12	2.17×10^{-1}	3.44 (360)
	1 → 23	1.32×10^{-1}	4.08 (304)
	2 → 34	1.72×10^{-1}	2.62 (474)
	2 → 29	1.42×10^{-1}	2.40 (516)
	3 → 40	1.22×10^{-1}	2.71 (458)
2	1 → 15	2.69×10^{-1}	3.87 (320)
	2 → 20	1.99×10^{-1}	2.12 (585)
	2 → 25	1.94×10^{-1}	2.42 (513)
	3 → 29	9.88×10^{-2}	2.50 (496)
3	1 → 15	1.74×10^{-1}	3.83 (324)
	2 → 20	2.05×10^{-1}	2.10 (590)
	3 → 29	1.07×10^{-1}	2.46 (504)

[a]Initial (I) and final (F) singlet excited states. [b]Oscillator strengths in the length representation.

For the $S_0 \rightarrow S_1$ and $S_0 \rightarrow S_2$ transitions in **1** and **2**, the dominant NTOs obtained by the TD-CAM-B3LYP(+PCM) method (Figures S16 and S17 in the SI) are analogous to the ADC(2)/cc-pVDZ ones.[22] The character of the dominant NTOs already anticipates the anti-Kasha photochemistry; namely, why it is difficult for the C−N bond to survive the transition to S_2. In this state, the π(C−N) bonding interaction is depleted of its charge density, which is transferred toward the benzene ring(s) and/or the π(N−N) bond (Figure S17 in the SI). Consequently, we observed that the attempts at optimizing the S_2 minimum fail when the structure becomes stuck in the vicinity of the conical intersection (CI) that precedes the elimination of the nitrogen. Prior to the elimination, the N_2 moiety assumes the direction quasi-perpendicular to the benzene ring. This observation is in line with the deactivation of the S_2 state in **1** and **2** via locally nonplanar conformations of the CI, as was observed in the nonadiabatic MD runs.[22]

In the S_1 state, the charge is transferred mainly locally within the C−N−N π-system. While this also weakens the C−N bond, the effect is less pronounced than that in S_2. Consequently, it is possible to optimize stable S_1 minima of **1**, **2**, and **3**. In these minima, the C−N bond is on average elongated by 0.07 Å relative to the ground state and the N_2 moiety is tilted (the C−N−N angles are ∼130°; Figure 2). However, unlike the situation in S_2, the diazo group remains bonded to the C atom (although the bond length now approaches that of the single C−N bond), and its axis remains more aligned with the benzene ring plane; the corresponding angles equal 33° (**2**) and 19° (**3**). This also agrees with the findings from the nonadiabatic MD runs, which indicated that the radiationless decay of S_1 takes place predominantly via locally quasi-planar conformations of the S_1/S_0 CI.[22]

The T_1 minima of **1**, **2**, and **3** show similar features as the S_1 minima; namely, the weakened but preserved C−N bond and the tilted N_2 moiety (Figure 2). The T_1 states of **2** and **3** absorb in the 400−420 nm region (vide infra), which can be correlated to the TD-CAM-B3LYP-computed lowest transitions at 402 (**2**) and 478 (**3**) nm. This wavelength difference is attributable to the notable difference in conformations of **2** and **3** in the T_1 state; in **2**, the N_2 and benzene chromophores close the angle of ca. 70°, while in **3** this angle is only ca. 30°. Although typically produced via inefficient intersystem crossings (ISC), the long-lived T_1 states are of interest as alternative precursors to the triplet carbenes, which may in turn explain the observed ketone photoproducts.

Focusing on the spectra of the singlet and triplet **car-1−3** transients, the used TD-CAM-B3LYP and CASPT2 methods here exhibit some important differences (Figures S18−S20 in the SI). For the singlet carbenes, TD-CAM-B3LYP predicts the strongest maxima as considerably blue-shifted and completely overlooks the significant features in the region of ca. 350−450 nm, which disagrees with the experimental TA data (vide infra). The spectra of the triplet carbenes agree better for **car-2** and **car-3**, but the discrepancies remain for **car-1**. Additionally, TD-CAM-B3LYP generally predicts much larger oscillator strengths than CASPT2. Considering the extensively documented multiconfigurational nature of carbenes,[50] we consider the CASPT2 spectra to be more reliable even though there could be somewhat larger uncertainties in the oscillator strengths, which are presently computed as the

https://doi.org/10.1021/acs.joc.2c02875
J. Org. Chem. 2023, 88, 4286−4300

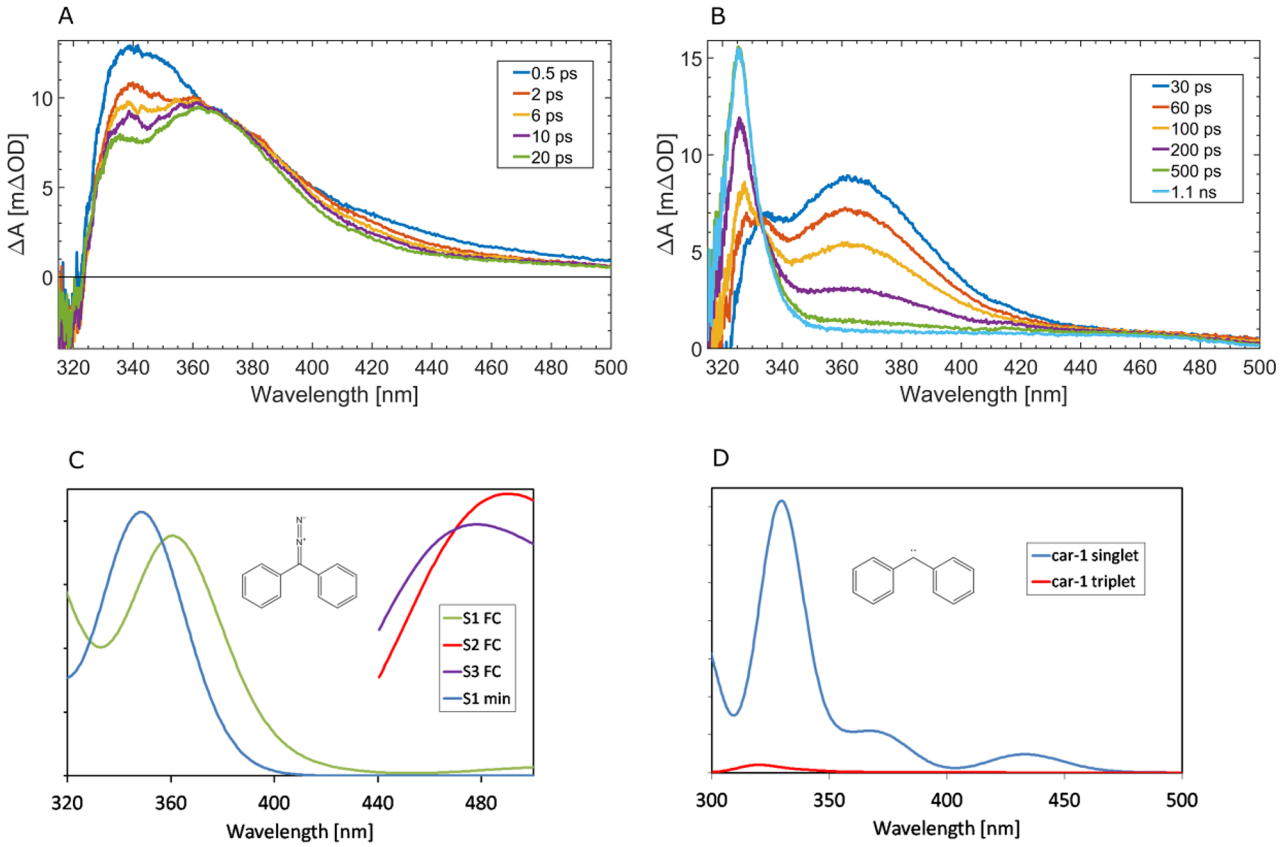

Figure 4. (A) Transient absorption spectra of **1** upon excitation at 267 nm at early times. (B) Later transient absorption spectra of **1** at up to 1.1 ns probe delay. (C and D) Excited-state absorption spectra computed for **1** and **car-1**. "S_1 FC" and "S_2 FC" were computed at the ground-state (S_0) minimum, while "S_1 min" was computed at the S_1 minimum. The spectra are convoluted with the Gaussian profiles (fwhm = 3000 cm^{-1}).

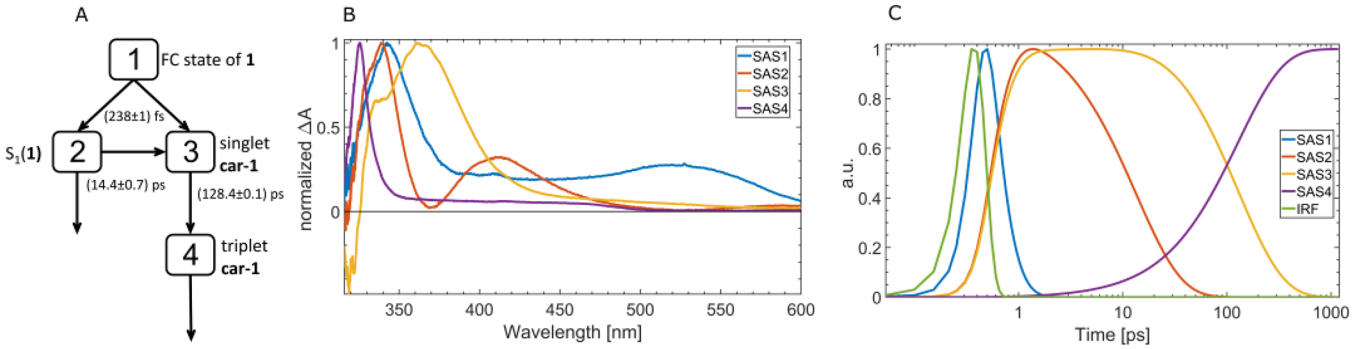

Figure 5. (A) Model for the target analysis of **1** that produced the best global fit results. (B) Species-associated spectra (SAS) corresponding to the four compartments of the target model of **1**. (C) Normalized time profiles of the species-associated spectra and instrument response function for the corresponding target analysis model, shown in a logarithmic time scale.

dipole moment expectation values between the uncorrelated (CASSCF) wave functions.

Ultrafast Transient Absorption Spectroscopy. fs-TA measurements for **1** in different solvents have been reported.[38,43] We conducted fs-TA measurements for **1**−**3** in cyclohexane, upon excitation at 267 nm, which populates higher singlet excited states, S_2 and S_3 (the Franck−Condon states, FC), and we particularly focus on the early events after the excitation. The corresponding spectra are shown in Figures 4, 6, and 8. Global and target analysis of the transient data (using GloTarAn software[51]), as well as single wavelength fitting, was performed to extract characteristic time constants and to aid in data interpretation. To assign the bands in the fs-TA spectra of **1**−**3**, we conducted computations of the ESA spectra for **1**−**3**, as well as the spectra of the corresponding singlet and triplet carbene intermediates. The comparison of our spectra for **1** and those in precedent literature[38,43] with the computed ones can serve as a benchmark to verify the validity of the level of theory used.

In the fs-TA spectra of **1**, at early times (<1 ps), a transient absorption spectrum was detected with a clear maximum around 340 nm and broad absorption stretching over almost the whole visible region (Figure 4A). The early transient spectrum decays within the temporal resolution of our setup with a 238 fs time constant, revealing the absorption of another species with maxima at 335 nm and around 360 nm. Two

https://doi.org/10.1021/acs.joc.2c02875
J. Org. Chem. 2023, 88, 4286−4300

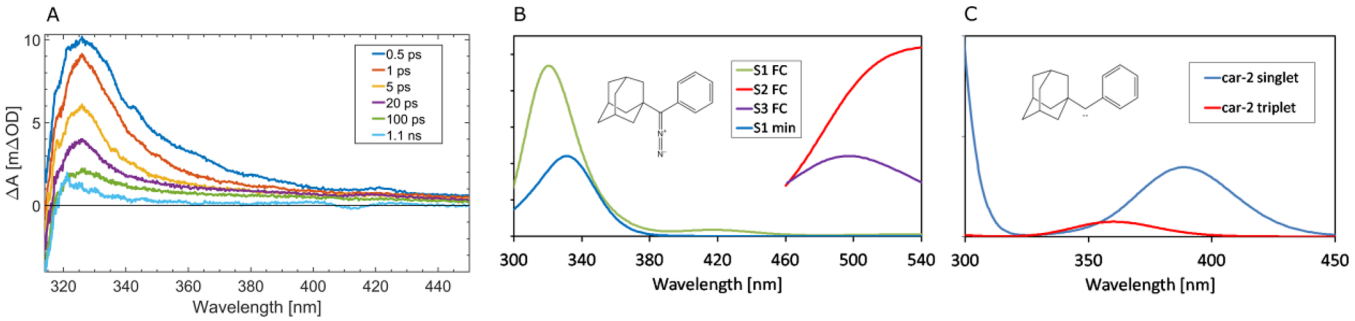

Figure 6. (A) Transient absorption spectra of **2** upon excitation at 267 nm. (B and C) Excited-state absorption spectra computed for **2** and **car-2**. "S_1 FC" and "S_2 FC" were computed at the ground-state (S_0) minimum, while "S_1 min" was computed at the S_1 minimum. The spectra are convoluted with the Gaussian profiles (fwhm = 3000 cm^{-1}).

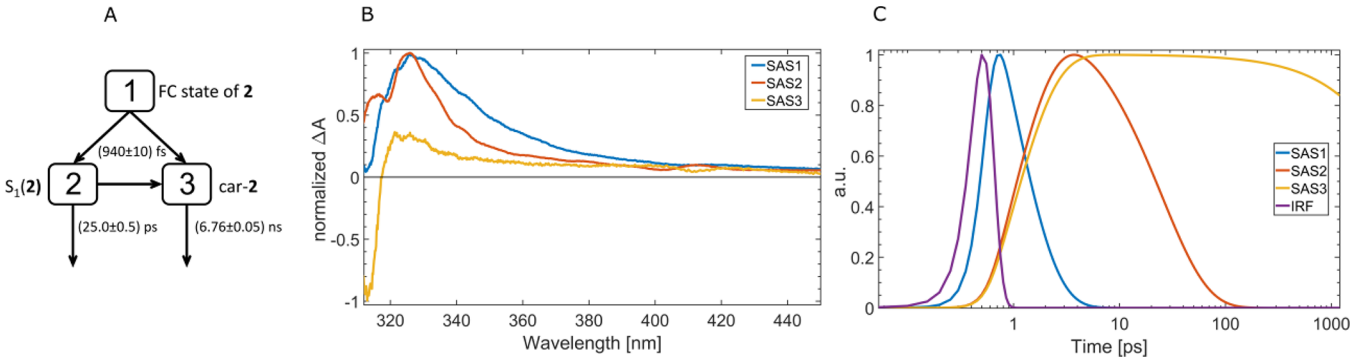

Figure 7. (A) Model for the target analysis of **2** that produced the best global fitting results. (B) Species-associated spectra (SAS) corresponding to the three compartments of the target model of **2**. (C) Time profiles of the species-associated spectra and instrument response function for the corresponding target analysis model, shown in a logarithmic time scale.

decay constants, 14.4 and 128.4 ps, describe the dynamics for both these peaks. A longer time constant coincides with the rise of the long-lived positive feature at 325 nm detected at later delay times (Figure 4B).

The model used for the target analysis and its results for fs-TA spectra of **1** (Figure 5) consists of four compartments (other tested models are shown in Figure S4). The species-associated spectrum of the first compartment (SAS1, Figure 5A) was assigned to the initially excited FC state of **1**, and it is in relatively good agreement with the calculated **1** (S_2) excited-state absorption (ESA) above 450 nm shown in Figure 4C. Here we note the similar assignment of this broad spectrum to initially excited singlet state absorption in other fs-TA experiments.[39]

Two new species are formed from the FC state in parallel processes. The shoulder at 360 nm, already observed after 1 ps, corresponds to the singlet carbene formed from **1**, **car-1** (compartment 3). The signal around 335 nm was assigned to the relaxed S_1 state of molecule **1** due to overlapping of SAS2 and the calculated spectrum of the relaxed S_1 state. Most of the **car-1** population is formed from the initially excited FC state of **1**, but a small part could be formed through the inefficient photoelimination of nitrogen via a locally planar conical intersection (CI) from the relaxed S_1 state of **1**, as was also suggested by computations.[22] The formation of **car-1** from the relaxed S_1 was included in our model, as it resulted in increased quality of the global fit.

The relaxed S_1 state further decays into ground state of **1** (14.4 ps). The singlet carbene decays with the time constant of 128.4 ps, forming new species absorbing at 325 nm, with a clear isosbestic point in the fs-TA spectra around 330 nm. The species absorbing at 325 nm was assigned to the triplet carbene from **1**, and the rate constant for its formation is in line with precedent literature for the intersystem crossing (ISC) in diphenylmethylene in nonpolar solvents.[38,39] The decay of triplet **car-1** could not be resolved in our fs-TA measurements. By comparing measured and calculated spectra shown in Figure 4, it can be seen that for singlet carbene there is substantial difference in the spectral shape, where only a minor peak in the calculated spectra around 370 nm corresponds to our measurements. Here we note that calculated oscillator strengths are less reliable than corresponding spectral positions, and it is possible that the maximum around 430 nm, which we do not observe experimentally, is much weaker than the one at 370 nm, which coincides with the measured spectra assigned to singlet **car-1**. The maximum around 335 nm could be overlapped with ESA from **car-1** in the triplet state, and its amplitude could be much weaker than the calculated value as well. In addition, the calculated maxima for singlet-state carbene generally appear at longer wavelengths compared to the triplet, which is in good agreement with the experimental data.

In the fs-TA spectra of **2**, at an early time after the 267 nm excitation, the transient absorption is detected with a maximum at 326 nm and shoulders stretching to 450 nm (Figure 6A). We assume that this early absorption spectrum corresponds to initially excited S_2 FC state of **2**. As it is also the case for **1**, the computations of the ESA spectra from the S_2 and S_3 FC states of **2** predict intense features in the visible range (450 nm and above). We note that the modeled S_2 and S_3 spectra are cut off at the onset of the first ionization threshold, i.e., some 2.7−2.8 eV above S_2/S_3. Fast dynamics of

https://doi.org/10.1021/acs.joc.2c02875
J. Org. Chem. 2023, 88, 4286−4300

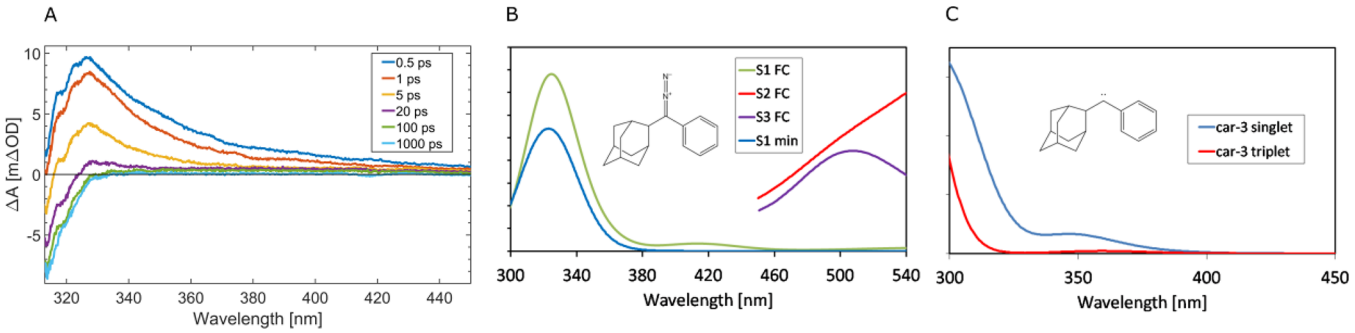

Figure 8. (A) Transient absorption spectra of **3** upon excitation at 267 nm. (B and C) Excited-state absorption spectra computed for **3** and **car-3**. "S_1 FC" and "S_2 FC" were computed at the ground-state (S_0) minimum, while "S_1 min" was computed at the S_1 minimum. The spectra are convoluted with the Gaussian profiles (fwhm = 3000 cm^{-1}).

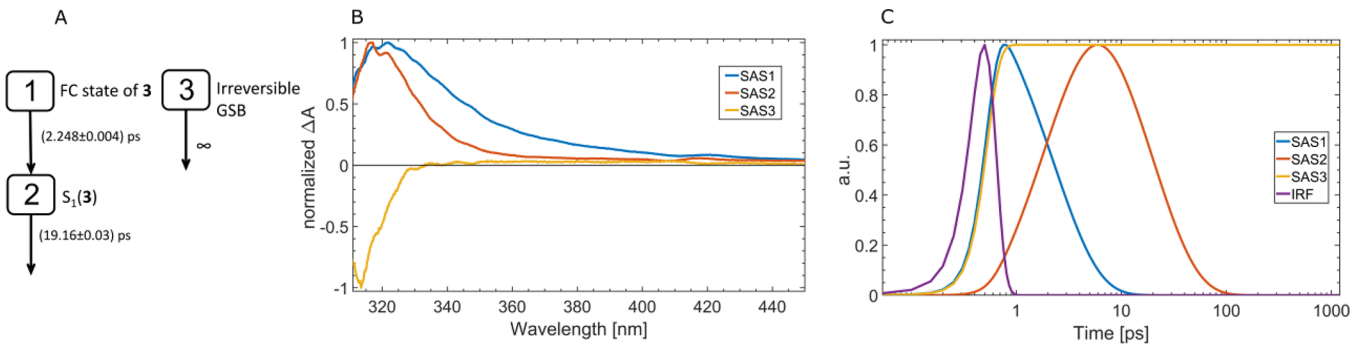

Figure 9. (A) Model for the target analysis of **3** that produced the best global fitting results. (B) Species-associated spectra (SAS) corresponding to the four compartments of the target model of **3**. (C) Time profiles of the species-associated spectra and instrument response function for the corresponding target analysis model, shown in a logarithmic time scale.

the fs-TA spectra of **2** is described with biexponential decay. Extracted time constants are 940 fs and 25 ps. After the initial fast decay, the measured spectrum consists of a negative signal at ≈300 nm due to irreversible ground-state bleach of molecule **2** and a positive signal with a maximum around 320 nm.

The model consisting of three compartments that was used in the target analysis of the measured data is shown in Figure 7. We assign the broad spectra of SAS1 to the initially populated FC state of **2**. It decays with the time constant of 940 fs and populates compartments 2 and 3 that correspond to **2** (S_1) and singlet carbene (**car-2**), respectively. SAS2 is in good agreement with the computed ESA of **2** (S_1 min) depicted in Figure 6B. The model allows for the additional (inefficient) formation of singlet carbene from the **2** (S_1) state. Since the ground-state bleach is irreversible and the decay of the third compartment is much longer than the available time delay window, they are both represented in SAS3. While it is expected that singlet carbene formation occurs in parallel processes from the FC state,[22] there is a significant discrepancy between the calculated spectra peaking at 390 nm and very broad SAS3 having a maximum at a much shorter wavelength around 325 nm.

Alternative interpretation of the compartments matches SAS3 to the ESA of the triplet excited state **2** (T_1), whereas both **car-2** and **2** (S_1) would be represented by the second compartment with significant spectral overlap and similar temporal decay. It is anticipated that the triplet excited state can be populated via ISC from both the FC state and **2** (S_1). However, since ISC is a spin-forbidden process, it is expected to take place mainly from the relaxed S_1 state, as it should be slower compared to IC from the FC state to the relaxed S_1, which does not fit well with the model represented in Figure 7. Moreover, it should be noted that LFP measurements detected **2** (T_1) absorbing at longer wavelengths around 420 nm (vide supra), rendering the assignment of compartment 3 to **2** (T_1) less likely. Consequently, the best fit of the global model to the experimental data corresponds to the assignment of compartment 2 to **2** (S_1) and that of compartment 3 to **car-2**. Furthermore, the largest part of **car-2** is formed directly from the FC state in the anti-Kasha photochemical reaction.

The fs-TA spectra of **3** (Figure 8A) are similar to those from **2**. Both samples exhibit biexponential fast decay of the positive absorption bands and a long-lived negative ground-state bleach signal. However, there is an important distinction. By comparing the TA spectra at the longest delay point, it can be seen that in **2** there is still some positive signal above 320 nm that is not present in **3**. We used three compartments to describe the data using global target analysis (Figure 9). Spectra belonging to first two compartments correspond to the initially excited FC state and the relaxed singlet excited **3** (S_1) state. Dynamics of these states are described by 2.2 ps decay for the FC state and 19.2 ps decay for the S_1 state. The spectral position of **3** (S_1) agrees with the calculated ESA of **3** (S_1) from Figure 8B. The third compartment in target analysis was introduced to describe the long-lived ground state bleach that indicates an additional pathway of the photoreaction from the initially excited state. Based on the identification of photoproducts (vide infra), we suspect that it corresponds to the irreversible formation of stable alkene **15** that does not absorb at 300 nm. Results of global analysis using another (parallel) model that produced reasonably good fitting results are shown in Figure S5 in the SI. The negative signal observed in the fs-

https://doi.org/10.1021/acs.joc.2c02875
J. Org. Chem. 2023, 88, 4286−4300

TA spectra could in principle correspond also to the stimulated emission from the higher excited state of **3**. However, the detected fluorescence spectrum of **3** stretches to 420 nm (Figure S2 in the SI), whereas the negative signal in the fs-TA was observed at λ < 350 nm, indicating that it is due to the ground-state bleach. The stimulated emission was probably not detected due to its low intensity and overlap with the positive transient absorption.

Note that the negative signal is (according to the global fit) formed at early times after the excitation, within the resolution of the setup. This indicates that the formation of **car-3** and subsequent H-insertion to **15** take place ultrafast from the initial FC state in another anti-Kasha photochemical reaction. The other option is that **car-3** is never formed and that **15** is produced directly in the RIES process from the FC state of **3**. Most likely, **car-3** has a low absorptivity, as in the case of **car-2**, whose absorption band was covered by the absorption of **2** (S_1). Moreover, the anticipated short lifetime of the singlet **car-3**, due to formation of **15**, makes it difficult to detect by transient spectroscopy. Thus, detection of **car-3** remains elusive.

Laser Flash Photolysis. The photochemistry of **1** has been intensively investigated by both laser flash photolysis (LFP) and fs-TA.[31−42] To detect plausible longer-lived reactive intermediates in the photochemistry of **2** and **3**, we conducted LFP measurements. The experiments were performed upon excitation with a YAG laser at 266 nm in a pentane solution at rt or at −90 °C. The solution was purged with N_2 and O_2, where we expected that O_2 would quench triplet excited states and triplet carbenes (for all LFP data, see Figures S6−S14 in the SI). A photochemical reaction on a similar molecule **Nor-1** (Figure 10) has been investigated by Tomioka et al.[52] whereas

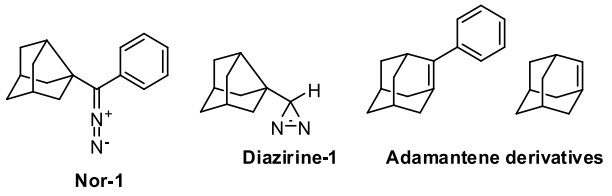

Figure 10. Diazo- and diazirine molecules and the corresponding intermediates investigated by Tomioka and Platz.[52,53]

Platz et al.,[53] studied the corresponding diazirine-1. Tomioka et al. detected a transient in degassed benzene absorbing at 430 nm that decayed, giving a new transient absorbing at 320 nm. The decay of the first transient with the lifetime of τ = 5.6 ms was correlated with the rise of the second transient absorbing at 320 nm, decaying over a much longer time scale. They assigned the primary transient at 430 nm to 1-phenyl-adamantene, whereas the transient at 320 nm was assigned to a dimerization product of 1-phenyladamantene (Figure 10). On the other hand, Platz et al. observed only one transient absorbing at 320 nm, assigned to adamantene, that decayed over millisecond time-scale but not with unimolecular kinetics.[53] For both anti-Bredt olefins, the rate constants with different quenchers were reported, including O_2 (10^6−10^7 M^{-1} s^{-1}) and CH_3OH (10^2−10^4 M^{-1} s^{-1}).[52,53]

In the N_2- and O_2-purged pentane solution of **2** (Figure S6 in the SI), two transients were detected, similar to the results of Tomioka et al. However, the transients decayed over a much shorter time scale (Figure S7 in the SI). The first transient was formed within the laser pulse. It had a lifetime of 750 ± 100 ns (k = 1.3 × 10^6 s^{-1}) and absorbed in the region 300−600 nm with a maximum at ≈400−420 nm. Its decay took place during the rise of the second transient absorbing at shorter wavelengths with a maximum at ≈350 nm. The rise of the second transient was faster (k = 3.3 ± 0.2 × 10^6 s^{-1}) than the decay of the first. The second transient had longer lifetime of 10−15 μs (Figure 11). After the decay of both transients, residual absorption was detected, probably corresponding to the formation of stable azine product absorbing over the whole spectrum.

In the O_2-purged pentane solution of **2**, the first transient (420 nm) was quenched and had the lifetime of 45 ± 10 ns (for the spectra in the presence of quenchers see Figures S8 and S9 in the SI). Taking the value of O_2 solubility in pentane at 20 °C of 17.7 × 10^{-3} M,[54] the shortening of the lifetime corresponds to k_q of 1.2 × 10^9 M^{-1} s^{-1}. This rate constant is similar to the values for the quenching of triplet excited states and triplet carbenes by O_2, whereas singlet carbenes react with O_2 slower with the rate of k ≈ 10^7 M^{-1} s^{-1}.[5] Note that the characteristic signal of carbon monoxide usually observed by the quenching of carbenes by O_2 was not detected.[34] The second transient (320 nm) was not quenched with O_2. A LFP experiment in the presence of pyridine, a ubiquitous carbene quencher, could not be performed due to the absorption of pyridine at 266 nm. Methanol is a good quencher of singlet carbenes (k_q= 10^8−10^9 M^{-1} s^{-1}) and triplet carbenes (k_q= 10^5−10^7 M^{-1} s^{-1}).[4,5] However, CH_3OH did not quench the first transient (420 nm). In the N_2-purged solution, in the presence of 0.1 M CH_3OH the lifetime of the first transient was even slightly longer (850 ± 100 ns). On the contrary, in the presence of CH_3OH the second transient (320 nm) was not detected, suggesting that its formation involved carbene intermediates and presumably did not involve the first transient (420 nm). Based on the above discussion, the first transient (420 nm) was tentatively assigned to the triplet excited state of **2**. This triplet excited state is most likely not involved in the formation of products reported in literature precedent,[22] except ketone. Based on the work of Tomioka[52] and Platz,[53] the second transient (320 nm) is tentatively assigned to an anti-Bredt olefin, product **16** (Scheme 3).

In the N_2-purged pentane solution of **2** at −90 °C, two transients were detected (Figures S13 and S14 in the SI). The first is short-lived, τ = 300 ± 100 ns, and absorbs in the region 320−400 nm. The other transient is longer-lived and absorbs almost over the whole spectrum with a maximum at 400−420 nm. The lifetime of the second transient is 5.2 ± 0.2 μs. Its formation could be time-resolved; it was formed with the rate constant of k = 7 ± 2 × 10^6 s^{-1}. Contrary to the pentane solution at rt, very long-lived transient that was assigned to olefin **16** was not detected (maximum at 350 nm, τ = 10−15 μs). In O_2-purged solution, only a very weak transient was detected at 400−420 nm with the lifetime of ≈30 ns. From the lifetimes in N_2- and O_2-purged solution rate constant for the quenching of long-lived transient at 400−420 nm is k_q ≈ 2 × 10^9 M^{-1} s^{-1}. Based on the study at −90 °C, quenching with O_2, and computations, the transient with the lifetime of 300 ns detected at −90 °C only was tentatively assigned to the triplet state of **car-2**, whereas the transient with the lifetime of 5 μs probably corresponds to the triplet excited state of **2**.

In the N_2- and O_2-purged pentane solution of **3** (Figure S11 and S12 in the SI), a transient was observed absorbing at 300−550 nm with a maximum at 400−420 nm. Its formation could not be time-resolved; it took place during the laser pulse. The

https://doi.org/10.1021/acs.joc.2c02875
J. Org. Chem. 2023, 88, 4286−4300

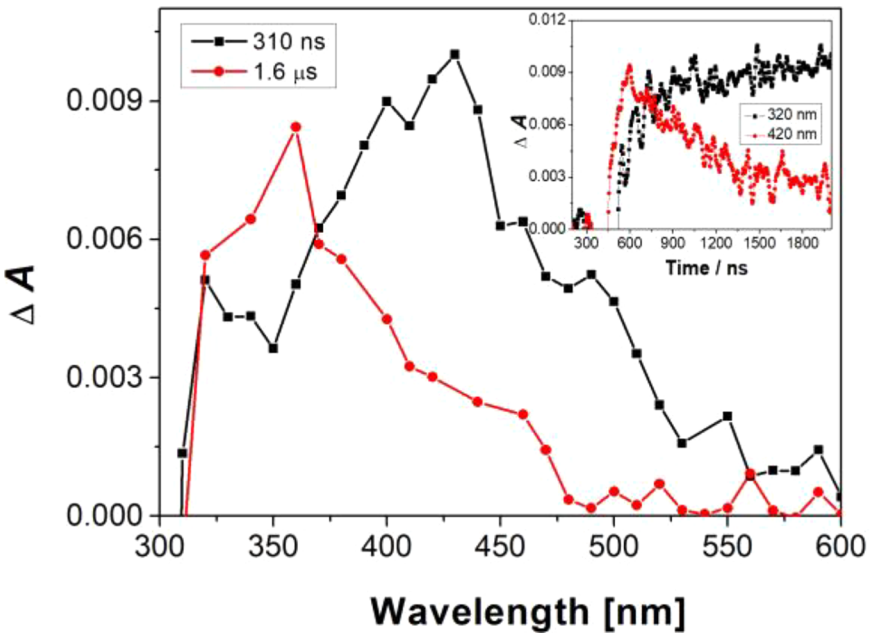

Figure 11. Transient absorption spectra of **2** ($c = 1.83 \times 10^{-4}$ M) in a N_2-purged pentane solution (at rt) with a delay of 310 ns, or 1.6 μs after the laser pulse (266 nm). The inset shows the growth kinetics at 320 nm and decay kinetics at 420 nm.

Scheme 2. Photochemical Pathways of 1

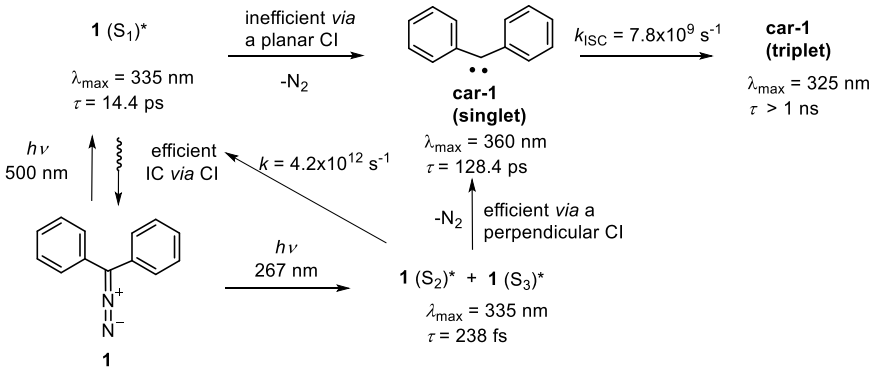

Scheme 3. Photochemical Pathways of 2

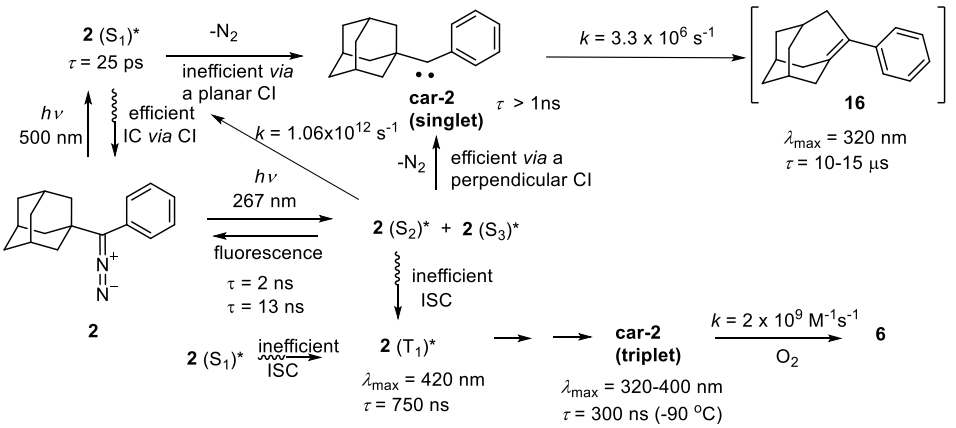

decay of the transient in N_2-purged solution followed unimolecular kinetics with the lifetime of 1.0 ± 0.1 μs. The decay of the transient was faster in the O_2-purged solution with the lifetime of 120 ± 10 ns, which roughly corresponds to $k_q \approx 4.1 \times 10^8$. Based on the findings for **2**, the transient was tentatively assigned to the triplet excited state of **3**. After the decay of the triplet, no additional longer-lived transient was observed. However, absorption spectra after LFP (Figure S10 in the SI) indicate the formation of a stable product with an absorption band at shorter wavelengths, ca. 250 nm. This

https://doi.org/10.1021/acs.joc.2c02875
J. Org. Chem. 2023, 88, 4286−4300

Scheme 4. Photochemical Pathways of 3

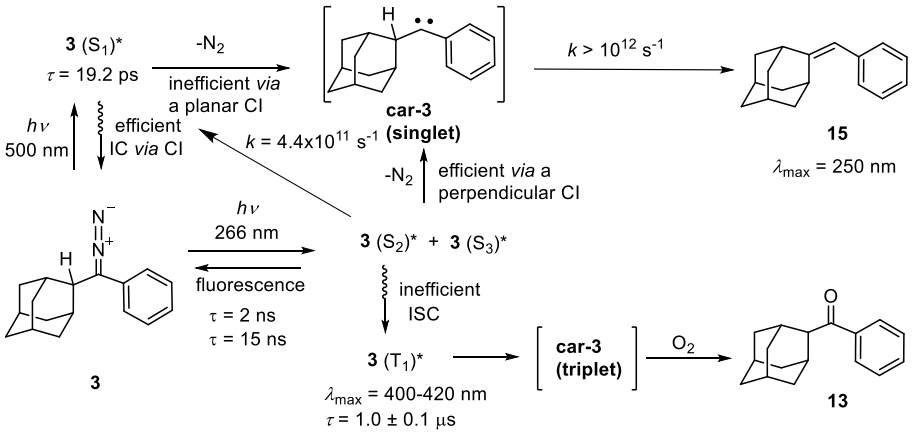

absorption corresponds to photoproduct **15** formed by the C−H insertion, which was isolated and fully characterized. **car-3** was not detected. However, the isolation of ketone **13** strongly indicated that it was formed via triplet carbene **car-3**.

Reaction Mechanisms. Based on previous discussion, in Scheme 2 we present reaction pathways of **1**. UV pulses at 267 nm excite the initial molecule to the S_2 and S_3 FC states. From there, the nitrogen elimination reaction takes place, efficiently producing **car-1** in the singlet state via locally perpendicular CI.[22] This confirms that the formation of **car-1** falls under anti-Kasha photochemisty. The initially excited FC state of **1** also goes through IC to the **1** (S_1) state, which further relaxes to the ground state of **1** through efficient IC via conical intersection. **car-1** can also be formed inefficiently from **1** (S_1) via a locally planar CI.[22] Singlet carbene undergoes ISC with a 128.4 ps time constant to the ground triplet state, which is more stable by 5.3 kcal mol^{-1} according to the CASPT2 method (vide supra). Both carbene species can be intercepted with different reagents/molecules, which was studied in detail in previous literature.[32−43]

The light excitation of **2** at 267 nm populates the S_2 and S_3 FC states, which relax to S_1 with a time constant of 940 fs. Concomitantly, in the competing photochemical reaction taking place from the FC state, the elimination of nitrogen via CI takes place, delivering **car-2** in the singlet state (Scheme 3). The time resolution for the N_2 elimination could not be resolved from the IC process delivering **2** (S_1), but there is an undeniable evidence that **car-2** is mainly formed directly from the FC state of **2** in the ultrafast reaction. Thus, the elimination of N_2 is much more facilitated from the S_2 or S_3 state than from S_1. In the case of **2**, fs-TA spectra did not reveal an ISC process from the singlet **car-2** to the triplet. The singlet carbene deactivates by insertion into the C−C bond of adamantane, giving anti-Bredt olefin **16**, tentatively detected by LFP, and it reacts with the solvent in a bimolecular reaction to deliver C−H insertion products, which were documented previously.[22] Thus, singlet carbene **car-2** has longer lifetime, most probably in the range of 1−10 ns, which cannot be measured by our fs-TA or ns LFP setups. Note that the energy difference between the singlet and triplet carbenes is the largest among those investigated. Thus, ISC process in this case is the slowest and in competition with the unimolecular C−C insertion reaction or bimolecular C−H insertion with the solvent.

Table S6 shows the computed rate constants and reaction free energies for the insertion of the singlet **car-2** into the adjacent C−C bond. Figure S21 depicts the corresponding transition state and product **16** optimized at the CAM-B3LYP(+PCM)/6-311+G(2d,p) level. The rate constant for this reaction computed using the hybrid meta-GGA density functional M06 ($k = 1.2 \times 10^6$ s^{-1}) is in the best agreement with the measured value of 3.3×10^6 s^{-1} (Scheme 3). This is in line with our previous findings, viz., in the DFT/PCM setting, hybrid GGA functionals (e.g., M06, PBE0 and B3LYP) perform better for the activation barriers and rate constants than range-separated hybrids.[55] The reaction free energies are in good agreement for all the tested functionals with the estimated value of −36 ± 2 kcal mol^{-1}.

The singlet excited state of **2** (the FC state or relaxed S_1) also undergoes inefficient ISC, populating the triplet excited state of **2**, which was detected by LFP. Most likely, the formation of the triplet carbene **car-2**, detected by LFP at −90 °C, can be rationalized as species formed from **2** (T_1). The formation of the adamantyl phenyl ketone photoproduct is also a strong indication of the involvement of triplet carbene **car-2** in the photochemistry of **2**.[22] Thus, LFP and fs-TA allowed for the detection of both singlet and triplet carbene **car-2**, whereas fs-TA aksi showed evidence that N_2 elimination from **2** takes place from the FC state in the anti-Kasha photochemical reaction.

Due to the same type of chromophore in **2** and **3**, one would expect similar photophysical properties and photochemical pathways in early times after the 267 nm excitation. The early FC spectra computed for **2** and **3** (Figures 6 and 8) show only minor differences. These are mainly due to the differences in the minimum conformations, specifically the mutual positions of the phenyl and N_2 chromophores. Similar to the observed pathways for **2**, after the population of the FC state upon light absorption at 267 nm, the system deactivates by IC to the relaxed **3** (S_1) and by N_2 elimination to deliver **car-3**, which is expected to react via the insertion into the α-C−H bond to furnish the stable photoproduct alkene **15** (Scheme 4). The reaction, which can also be thought of as a hydrogen atom transfer from the α-C to the carbene C, is characterized by an early transition state (Figure S21 in the SI); hence, it is exceedingly fast and exothermic with a CAM-B3LYP rate constant of >10^{12} s^{-1} ($\Delta G^{\ddagger}$ = 1.3 kcal mol^{-1}) and a reaction free energy of −67 kcal mol^{-1}. Thus, although the singlet **car-3** exists as a minimum on the free-energy surface, it is very shallow and fleeting, with an upper lifetime bound at 298 K in the subpicosecond time scale. Indeed, the facile torsion around

https://doi.org/10.1021/acs.joc.2c02875
J. Org. Chem. 2023, 88, 4286−4300

the >C(H)−$C_{carbene}$ bond approximates the reaction coordinate well; the relaxed scan with respect to this mode is sufficient to trigger the rearrangement of the singlet **car-3** to the photoproduct **15**. This, in addition to its low absorptivity, precludes its detection by the fs-TA.

On the other hand, photoproduct **15** might form directly from the FC state of **3** in the RIES process, thus circumventing the carbene species. Since the negative bleach signal due to the irreversible formation of **15** is detected at very early times after the excitation in parallel to the relaxation to **3** (S_1), our experiments strongly indicate that it is another example of the anti-Kasha photochemical reaction. The relatively large energy gap between S_2 and S_1 (see the SI) allows for the competing IC and photochemical pathway to deliver **car-3** or **15**.

While we have no spectroscopic evidence for the formation of the singlet **car-3**, the isolation of ketone **6** in the photochemistry of **3** is a strong indication that triplet **car-3** was present in the photochemical reaction. According to the CASPT2 method, the triplet **car-3** is 7.3 kcal mol^{-1} more stable than the corresponding singlet. It is most likely formed from the triplet excited state of **3**, which was detected by LFP. The triplet excited state of **3** can be formed from the FC state of **3** or from the relaxed S_1 state. Although we did not detect the triplet carbene **car-3**, it should have a longer lifetime compared to that of the singlet since it should not undergo synchronous α-C−H insertion. The lack of triplet **car-3** detection is probably due to its inefficient formation. Overall, after the excitation of **3** at 267 nm, the main pathway involves anti-Kasha singlet reactivity, delivering stable photoproduct **15**.

As discussed above, the singlet−triplet ISC of **car-1**−**3** can compete with their reactions with the solvent and intramolecular rearrangements. However, our attempts at computing the corresponding ISC rates using the path integral formalism[56] failed. This is presently caused by the observed breakdown of the harmonic FCHT approximation (indicated by the too large values of the norm of the displacement vector in the Duschinsky transformation). We still note that, because of the significantly smaller S−T gap in **car-3**, the ISC rate from **car-3** should be significantly faster than that from **car-2** due to both compounds having comparable spin−orbit couplings. Still, due to the ultrafast α-C−H insertion in **car-3** the ISC yields should be negligible compared to the formation of the alkene **15**.

Finally, the computations provided some hints as to the conceptually and practically important reactivity of the studied diazo compounds and their photochemical transients in excited states, especially with regard to the possibility of the RIES. The S_2 state is again confirmed as an efficient precursor to the elimination of N_2, since the attempts at optimizing the S_2 minima of **1**, **2**, and **3** with the C−N bond preserved were unsuccessful. To estimate the feasibility of the N_2 elimination from the S_1 and T_1 states, beginning with the S_1 and T_1 minima we performed relaxed surface scans by gradually extending the C−N bond. At the TD-CAM-B3LYP level, the C−N bond dissociation energies are similar for **2** and **3**, approximately 14 kcal mol^{-1} from S_1 (at which point the CI with the ground state is encountered) and 12−13 kcal mol^{-1} from T_1.

The conformational features of the structures from the relaxed scans do not furnish evidence that the N_2 elimination in the excited states might be concerted with the insertion into the α-C−H bond. Namely, the process of C−N bond dissociation in S_1 and T_1 is not accompanied by the torsion around the >C(H)−$C_{carbene}$ bond that would enable the concomitant α-C−H insertion (vide supra). The similar observation applies to the conformations in the vicinity of the CI that give rise to the N_2 elimination. We note, however, that the relaxed scans may diverge from the true reaction paths, so more reliable answers as to the possibility of the RIES could be obtained from nonadiabatic dynamics, although this has thus far been unfeasible due to the large size of the adamantyl derivative.[22]

CONCLUSION

Photochemical reactivities of diazo compounds **1**−**3** and the corresponding carbenes was investigated computationally using the methods of time-dependent density functional theory (TD-CAMB3LYP) and multiconfigurational perturbation theory to the second order, as well as experimentally by transient spectroscopy. We provide the first spectroscopic evidence that the elimination of N_2 from diazo compounds upon excitation at 267 nm takes place in the anti-Kasha ultrafast photochemical reaction, within 1 ps, directly from the upper excited singlet states. The singlet carbenes from **1** ($\lambda_{max} \approx 360$ nm, $\tau = 128.4$ ps) and **2** ($\lambda_{max} \approx 325$ nm, $\tau > 1$ ns) were detected by fs-TA. In addition, we detected triplet carbenes formed by ISC from **car-1** ($\lambda_{max} = 325$ nm, $\tau > 1$ ns) or by the elimination of N_2 from the triplet excited state of **2** ($\lambda_{max} = 325$ nm, $\tau > 1$ ns). The reactivity of singlet carbenes differs with respect to the substituent at the carbene center. In nonpolar solvents, they undergo ISC or insertion reactions into C−H and C−C bonds ($\lambda = 320$−400 nm, $\tau = 300 \pm 100$ ns at −90 °C). In particular, elusive singlet **car-3** should have a very short lifetime (upper limit of $\tau = 1$ ps) due to the presence of an α-C−H bond next to the carbene center and an intramolecular C−H insertion reaction. This spectroscopic evidence that sheds light on the mechanism of carbene formation is important because it indicates that excitation to higher singlet excited states drives the efficient process, contrary to the well-accepted paradigms in organic photochemistry. Moreover, the spectroscopic detection of different carbenes and rate constants for their reactions is important in planning reactivity and using such species in different processes, particularly in biology where the desired biological action can be in competition with numerous competing carbene pathways.

EXPERIMENTAL AND COMPUTATIONAL DETAILS

General details, synthetic procedures for the preparation of all known compounds, and a description of photochemical and photophysical experiments are provided in the SI.

Synthesis of 2-Adamantyl Phenyl Ketone Hydrazone (14). A solution of 2-adamantyl phenyl ketone (**13**) (1 mmol) and hydrazine monohydrate (20 mmol) in anhydrous MeOH (~10 mL) was refluxed for 24 h using an oil bath. The solvent was removed under reduced pressure, and the resulting solid was purified by column chromatography on silica gel (0−50% diethyl ether in hexane) to yield the corresponding hydrazone in the form of a colorless solid.

Colorless solid; isolated yield 30%; mp 138−140 °C (sublimes at 124−128 °C); ^{1}H NMR (300 MHz, $CDCl_3$) 7.40−7.47 (m, 2H), 7.31−7.38 (m, 1H), 7.17−7.23 (m, 2H), 5.01 (br.s, 2H), 2.73 (br.s, 1H), 2.07−2.18 (m, 2H), 2.03 (br.s, 2H), 1.79−1.93 (m, 4H), 1.69−1.78 (m, 4H),1.46−1.56 (m, 2H); ^{13}C{^{1}H} NMR (75 MHz, $CDCl_3$) δ 154.4, 134.5, 128.9, 128.1, 127.2, 50.6, 38.8, 37.7, 32.3, 29.5, 28.1, 27.9; IR (KBr) $\tilde{\nu}$ 3346 (m), 2904 (s), 2843 (m), 1442 (w), 740 (m), 689 (m) cm^{-1}; HRMS (ESI-TOF) m/z [M + H]+ Calcd for $C_{17}H_{22}N_2$ 255.1861, found 255.1855.

Synthesis of (2-Adamantyl)diazophenylmethane (3). To a suspension of a barium manganate ($BaMnO_4$, 8 mmol) and powdered

https://doi.org/10.1021/acs.joc.2c02875
J. Org. Chem. 2023, 88, 4286−4300

CaO (55 mmol) in dry diethyl ether (~5 mL) was added a solution of hydrazone **14** (1 mmol) in dry diethyl ether (~5 mL) under a nitrogen atmosphere. The reaction mixture was stirred at rt for 1 h. Filtration of solids and evaporation of the solvent under reduced pressure afforded the corresponding diazo compound.

Pink-colored waxy solid; isolated yield 98%; ^{1}H NMR ($CDCl_3$, 600 MHz) δ 7.32 (t, 2H, J = 7.9 Hz), 7.03 (t, 1H, J = 7.3 Hz), 6.97 (d, 2H, J = 7.9 Hz), 3.07 (s, 1H), 2.06 (br.s, 2H), 1.97−2.01 (m, 1H), 1.91−1.96 (m, 4H), 1.82−1.90 (m, 3H), 1.78 (br.s, 2H), 1.61 (d, 2H, J = 12.5 Hz); ^{13}C{1H} NMR ($CDCl_3$, 150 MHz): δ 131.7 (s, 1C), 128.8 (d, 2C), 123.4 (d, 1C), 122.6 (d, 2C), 38.5 (t, 2C), 38.4 (d, 1C), 37.4 (t, 1C), 32.6 (t, 2C), 29.8 (d, 2C), 27.8 (d, 1C), 27.1 (d, 1C), 1C not seen (C = N); IR (KBr) $\tilde{\nu}$ 2899 (s), 2847 (s), 2034 (s), 1596 (m), 1492 (m), 742 (m) cm^{-1}; UV cyclohexane λ_{max}/nm (log ε) 298 and 511 nm (4.21 and 1.55 M^{-1} cm^{-1}), benzene λ_{max}/nm (log ε) 292 and 514 nm (4.23 and 1.68 M^{-1} cm^{-1}); HRMS (ESI-TOF) m/z [M + H]+ Calcd for $C_{17}H_{21}N_2$ 253.1705, found 253.1716.

Femtosecond Transient Absorption. We investigated ultrafast dynamics of diazo derivatives on a homebuilt fs-TA experimental setup, which is detailed elsewhere.[57] Briefly, 120 fs pulses at an 800 nm center wavelength at a 1 kHz repetition rate were generated using a Ti:sapphire regenerative amplifier system (Spitfire, Spectra-Physics). For the pump pulses, the fundamental beam was frequency doubled to give 400 nm and then mixed with the leftover fundamental beam to produce 267 nm via sum frequency generation. Pump pulses were chopped at 500 Hz frequency using a synchronized mechanical chopper. Probe pulses were generated using a small amount of fundamental beam that passes through a delay line, which allows measurement up to ~1 ns. After the delay line, the beam was focused in a 3 mm thick CaF_2 crystal, producing a useful white light continuum spanning from 310 to 680 nm. The fundamental beam was eliminated from the probe beam using a high reflectivity mirror. The magic angle between pump and probe polarizations was achieved by rotating the probe polarization using a waveplate. Both beams were focused onto a 0.5 mm path length quartz flow cell that has two 0.2 mm thick aperture windows (48/UTWA2; Starna), which was used to minimize coherent artifacts in transient absorption spectroscopy. After passing through the flow cell, the probe beam is collimated and sent to a homemade spectrometer equipped with the detector (Hamamatsu S7030−1006) and read-out electronics capable of single-shot measurement of the probe spectrum at the full 1 kHz laser repetition rate (Entwicklungsbuero EB Stresing, Berlin, Germany). We determined a temporal resolution of 250 fs by fitting the Gaussian function and its time derivatives on coherent artifact signals obtained in measurements in pure solvent. In order to keep a reasonable signal-to-noise ratio, slightly higher pump fluences were used for adamantyl precursors **2** and **3**. Pump fluences were 1.13, 4.19, and 2.83 mJ/cm^2 for measurements on **1**, **2** and **3**, respectively.

Laser Flash Photolysis. All LFP measurements were performed on the University of Victoria setup, as previously described.[58] The samples were excited with a pulsed Nd:YAG laser at 266 nm (<50 mJ per pulse), with a pulse width of 10 ns. Static cells (7 mm × 7 mm or 10 × 10 mm) were used, and they were frequently exchanged to ensure no contamination with photoproducts. The solutions were purged with N_2 or O_2 for 20 min prior to performing the measurements. A Unisoku USP-203 cryostat placed at the position of the sample holder was used for the low temperature experiments.[59] Absorbances at 266 nm were 0.3−0.4. Details on the sample preparation for the LFP measurements can be found in the Supporting Information.

Computational Methods. The photochemistry of the studied compounds was modeled in the framework of density functional theory (DFT) and its time-dependent formalism (TD-DFT) using mainly the long-range corrected CAM-B3LYP hybrid density functional.[60] This functional has repeatedly been shown to reliably correct for the deficiencies of the parent B3LYP in the case of charge transfer and Rydberg excited states.[60,61] The S_0 and T_1 minima of the three diazo compounds (**1**, **2**, and **3**) and the corresponding singlet and triplet carbenes (**car-1**, **car-2**, and **car-3**) were optimized using the 6-311+G(2d,p) basis set. The lowest singlet excited state (S_1) minima of **1**, **2**, and **3** were optimized using the similarly sized minimally augmented Karlsruhe basis set ma-def2-TZVP(-f)[62,63] exploiting the resolution of the identity (RI) approach and auxiliary basis sets to accelerate the computations. Here, the nonlocal HF exchange term was evaluated using the chain-of-spheres (COSX) approximation, which increases the efficiency for hybrid density functionals.[64] The Coulomb term was fitted using the auxiliary def2/J basis set[65] and the split-RI-J scheme;[66] the COSX and RI-J schemes combined to give rise to the RIJCOSX approximation. In all the optimizations, the presence of the cyclohexane solvent was described in terms of the (conductor-like) polarizable continuum model (PCM);[67−69] see the SI for details on the DFT integration grids, used algorithms, and PCM molecular cavities. The equilibrium solvation was assumed in the optimizations and the nonequilibrium one in computing the absorption spectra (vide infra). The Grimme's G3 atom-pairwise dispersion correction based on the Becke−Johnson damping function (G3BJ) was used throughout.[70]

By optimizing the S_0 and S_1 minima of **1**, **2**, and **3** with the CAM-B3LYP(+PCM) method, we obtained a set of reasonable geometries at which we computed the ESA spectra to aid in the assignment of the relevant photochemical transients. The transition dipole moments between pairs of excited states were computed at the TD-CAM-B3LYP(+PCM)/ma-def2-TZVP(-f) level and were approximated as the expectation values of the dipole moment operator between the Kohn−Sham configuration interaction singles (CIS) (pseudo)wave functions resulting from the Tamm−Dancoff approximation.[71] At the ground state ("Franck−Condon", FC) geometries, as the initial states we considered S_1, S_2, and S_3, whereas at the S_1 minima we considered only the S_1 state. The ESA spectra were built on the basis of up to 45 calculated TD-DFT roots, which were sufficient to cover the spectral range of interest (300−700 nm, and up to the first ionization threshold in case of S_2 and S_3). For the pairs of the excited states involved in the most intense ESA transitions, the natural transition orbitals (NTOs) were analyzed.[72] To estimate the threshold energies for the formation of the radical cations, we computed the (gas-phase) vertical ionization potentials (IPs) of **1**, **2**, and **3** employing the electron propagator theory in the renormalized partial third order approximation (EPT-P3+)[73] with the Dunning's polarized valence triple-ζ cc-pVTZ basis set.[74]

The absorption spectra of singlet (spin-restricted) and triplet (spin-unrestricted) **car-1**, **car-2**, and **car-3** were computed at the TD-CAM-B3LYP(+PCM)/6-311+G(2d,p) level. In addition, we tried the single-state multiconfigurational perturbation theory to the second order (CASPT2).[75] To obtain the CASSCF reference wave functions, in the case of **car-1** we used the active space of 10 electrons in 10 orbitals (10,10), which is (4, 4) per each benzene ring and (2, 2) for correlating the carbene lone pair (the next larger active space would amount to (14, 14), which is too expensive). In the case of **car-2** and **car-3**, the (8, 8) active spaces were used, viz., (6, 6) on the benzene ring (i.e., the entire benzene π-system) and (2, 2) for the carbene lone pair. The cc-pVTZ basis set was employed for **car-1**, and the smaller cc-pVDZ was employed for **car-2** and **car-3**.[74] The 10 lowest state-averaged equally weighted CASSCF roots were considered. To mitigate the effects of intruder states, the imaginary level shift of 0.10 au was applied,[76] which proved beneficial in our previous studies.[77,78] The oscillator strengths are based on the expectation values of the dipole moment operator (the length representation) between the CASSCF references.[79] The CASPT2 spectra were computed for the gas-phase; in view of the small dielectric constant of the solvent cyclohexane, this is not expected to introduce major discrepancies relative to the solvated phase.

To investigate the intramolecular rearrangements and final products of the singlet **car-2** and **car-3**, the corresponding transition states and reaction activation energies were computed at the DFT(+PCM)/6-311+G(2d,p) level employing several density functionals (see SI). The rate constants for these reactions were estimated in the formalism of the transition state theory (TST) with the Wigner tunneling coefficient (WTC).

The following quantum chemistry codes were used: Gaussian 16, revision C.01[80] (the PCM-DFT optimizations and harmonic

https://doi.org/10.1021/acs.joc.2c02875
J. Org. Chem. 2023, 88, 4286−4300

frequencies of the S_0 states and transition states and the EPT-P3+ IPs), OpenMolcas 22.06[81] (the CASSCF/CASPT2 computations of the absorption spectra of the singlet and triplet **car-1**−**3**), and Orca 5.0.3[82,83] (the RIJCOSX-DFT(+CPCM) optimizations and harmonic frequencies of the S_1 minima, the ESA spectra, and the NTOs). The GaussView 5 program was used to visualize the NTOs.[84]

■ ASSOCIATED CONTENT

Data Availability Statement

The data underlying this study are available in the published article and its Supporting Information.

Supporting Information

The Supporting Information is available free of charge at https://pubs.acs.org/doi/10.1021/acs.joc.2c02875.

Detailed experimental procedures for the synthesis of known compounds; photochemistry, UV−vis and fluorescence data; fs-TA and LFP data; computational details; copies of ^{1}H and ^{13}C NMR spectra; and coordinates of the optimized molecular structures (PDF)

FAIR data, including the primary NMR FID files, for compounds **3** and **14** (ZIP)

■ AUTHOR INFORMATION

Corresponding Authors

Silvije Vdović − *Centre for Advanced Laser Techniques, Institute of Physics, 10 000 Zagreb, Croatia*; Email: silvije@ifs.hr

Ivan Ljubić − *Department of Physical Chemistry, Ruđer Bošković Institute, 10 000 Zagreb, Croatia*; Email: ivan.ljubic@irb.hr

Authors

Vedran Brusar − *Centre for Advanced Laser Techniques, Institute of Physics, 10 000 Zagreb, Croatia*

Mateo Forjan − *Centre for Advanced Laser Techniques, Institute of Physics, 10 000 Zagreb, Croatia*

Marija Aleškvić − *Department of Organic Chemistry and Biochemistry, Ruđer Bošković Institute, 10 000 Zagreb, Croatia*

Kristin Becker − *Department of Organic Chemistry and Biochemistry, Ruđer Bošković Institute, 10 000 Zagreb, Croatia;* Present Address: Zernike Institute for Advanced Materials, University of Groningen, Nijenborgh 4, NL-9747 AG Groningen, The Netherlands

Complete contact information is available at: https://pubs.acs.org/10.1021/acs.joc.2c02875

Notes

The authors declare no competing financial interest.

■ ACKNOWLEDGMENTS

These materials are based on work financed by the Croatian Science Foundation (HrZZ-UIP-05-2017-5831 to S.V., HrZZ-IP-2020-02-9932 to I.L., HRZZ-IP-2014-09-6312, and HrZZ-IP-2019-04-8008). The authors thank Cornelia Bohne for granting access to the VicPicK-CAMTEC facility for the experiments performed at the University of Victoria.

■ REFERENCES

(1) Hine, J. Carbon Dichloride as an Intermediate in the Basic Hydrolysis of Chloroform. A Mechanism for Substitution Reactions at a Saturated Carbon Atom. *J. Am. Chem. Soc.* **1950**, *72*, 2438−2445.

(2) von E. Doering, W.; Buttery, R. G.; Laughlin, R. G.; Chaudhuri, N. Indiscriminate Reaction of Methylene with the Carbon-Hydrogen Bond. *J. Am. Chem. Soc.* **1956**, *78*, 3224−3224.

(3) Moss, R. A.; Doyle, M. P. *Contemporary Carbene Chemistry*; Wiley, 2014.

(4) Jones, M., Jr.; Moss, R. A. Singlet Carbenes. In *Reactive Intermediate Chemistry*; Moss, R. A., Platz, M. S.; Jones, M., Jr., Eds.; Wiley, 2003; pp 273−328, and references cited therein.

(5) Tomioka, H. Triplet Carbenes. In *Reactive Intermediate Chemistry*; Moss, R. A., Platz, M. S.; Jones, M., Jr., Eds.; Wiley, 2003; pp 375−461, and references cited therein.

(6) Bourissou, D.; Guerret, O.; Gabbaï, F. P.; Bertrand, G. Stable Carbenes. *Chem. Rev.* **2000**, *100*, 39−91.

(7) de Frémont, P.; Marion, N.; Nolan, S. P. Carbenes: Synthesis, Properties, and Organometallic Chemistry. *Coord. Chem. Rev.* **2009**, *253*, 862−892.

(8) Hopkinson, M. N.; Richter, C.; Schedler, M.; Glorius, F. An Overview of *N*-Heterocyclic Carbenes. *Nature* **2014**, *510*, 485−496.

(9) Platz, M. S. A Perspective on Physical Organic Chemistry. *J. Org. Chem.* **2014**, *79*, 2341−2355.

(10) Moss, R. A. Adventures in Reactive Intermediate Chemistry: A Perspective and Retrospective. *J. Org. Chem.* **2017**, *82*, 2307−2318.

(11) Abdel-Wahab, A.-M. A.; Ahmed, S. A.; Dürr, H. Carbene Formation by Extrusion of Nitrogen. In *CRC Handbook of Organic Photochemistry and Photobiology*, 2nd ed.; Horspool, W. M., Lenci, F., Eds.; CRC Press: Boca Raton, FL, 2003.

(12) Nakamoto, K.; Ueno, Y. Diazirine-Containing RNA Photo-Cross-Linking Probes for Capturing micro RNA Targets. *J. Org. Chem.* **2014**, *79*, 2463−2472.

(13) Holland, J. P.; Gut, M.; Klingler, S.; Fay, R.; Guillou, A. Photochemical Reactions in the Synthesis of Protein-Drug Conjugates. *Chem. Eur. J.* **2020**, *26*, 33−48.

(14) Maas, G. New Syntheses of Diazo Compounds. *Angew. Chem., Int. Ed.* **2009**, *48*, 8186−8195.

(15) Black, T. H. The Preparation and Reactions of Diazomethane. *Aldrichimica Acta* **1983**, *16*, 3−10.

(16) Johnston, J. N.; Muchalski, H.; Troyer, T. L. To Protonate or Alkylate? Stereoselective Brønsted Acid Catalysis of C-C Bond Formation Using Diazoalkanes. *Angew. Chem., Int. Ed.* **2010**, *49*, 2290−2298.

(17) Padwa, A.; Weingarten, M. D. Cascade Processes of Metallo Carbenoids. *Chem. Rev.* **1996**, *96*, 223−269.

(18) Gutiérrez, S.; Tomás-Gamasa, M.; Mascareñas, J. L. Exporting Metal-Carbene Chemistry to Live Mammalian Cells: Copper-Catalyzed Intracellular Synthesis of Quinoxalines Enabled by N−H Carbene Insertions. *Angew. Chem., Int. Ed.* **2021**, *60*, 22017.

(19) Wang, J.; Burdzinski, G.; Gustafson, T. L.; Platz, M. S. Ultrafast Study of p-Biphenylyldiazoethane. The Chemistry of the Diazo Excited State and the Relaxed Carbene. *J. Am. Chem. Soc.* **2007**, *129*, 2597−2606.

(20) Yamamoto, N.; Bernardi, F.; Bottoni, A.; Olivucci, M.; Robb, M. A.; Wilsey, S. Mechanism of Carbene Formation from the Excited States of Diazirine and Diazomethane: An MC-SCF Study. *J. Am. Chem. Soc.* **1994**, *116*, 2064−2074.

(21) Arenas, J. F.; Lopez-Tocon, I.; Otero, J. C.; Soto, J. Carbene Formation in Its Lower Singlet State from Photoexcited 3H-Diazirine or Diazomethane. A Combined CASPT2 and ab Initio Direct Dynamics Trajectory Study. *J. Am. Chem. Soc.* **2002**, *124*, 1728−1735.

(22) Piteša, T.; Aleškvić, M.; Becker, K.; Basarić, N.; Došlić, N. Photoelimination of Nitrogen from Diazoalkanes: Involvement of Higher Excited Singlet States in the Carbene Formation. *J. Am. Chem. Soc.* **2020**, *142*, 9718−9724.

(23) Bogdanova, A.; Popik, V. V. Experimental and Theoretical Investigation of Reversible Interconversion, Thermal Reactions, and Wavelength-Dependent Photochemistry of Diazo Meldrum's Acid and Its Diazirine Isomer, 6,6-Dimethyl-5,7-dioxa-1,2-diaza-spiro[2,5]-oct-1-ene-4,8-dione. *J. Am. Chem. Soc.* **2003**, *125*, 14153−14162.

(24) Burdzinski, G.; Réhault, J.; Wang, J.; Platz, M. S. A Study of the Photochemistry of Diazo Meldrum's Acid by Ultrafast Time-Resolved Spectroscopies. *J. Phys. Chem. A* **2008**, *112*, 10108−10112.
(25) Nigam, M.; Platz, M. S.; Showalter, B. M.; Toscano, J. P.; Johnson, R.; Abbot, S. C.; Kirchhoff, M. M. Generation and Study of Benzylchlorocarbene from a Phenanthrene Precursor. *J. Am. Chem. Soc.* **1998**, *120*, 8055−8059.
(26) Bonneau, R.; Liu, M. T. H.; Kim, K. C.; Goodman, J. L. Rearrangement of Alkylchlorocarbenes: 1,2-H Shift in Free Carbene, Carbene-Olefin Complex, and Excited States of Carbene Precursors. *J. Am. Chem. Soc.* **1996**, *118*, 3829−3837.
(27) Burdzinski, G.; Wang, J.; Gustafson, T. L.; Platz, M. S. Study of Concerted and Sequential Photochemical Wolff Rearrangement by Femtosecond UV−vis and IR Spectroscopy. *J. Am. Chem. Soc.* **2008**, *130*, 3746−3747.
(28) Wang, J.; Burdzinski, G.; Kubicki, J.; Platz, M. S. Ultrafast UV-Vis and IR Studies of p-Biphenylyl Acetyl and Carbomethoxy Carbenes. *J. Am. Chem. Soc.* **2008**, *130*, 11195−11209.
(29) Burdzinski, G.; Zhang, Y.; Selvaraj, P.; Sliwa, M.; Platz, M. S. Direct Observation of 1,2-Hydrogen Migration in the Excited States of Alkyl Diazo Esters by Ultrafast Time Resolved IR Spectroscopy. *J. Am. Chem. Soc.* **2010**, *132*, 2126−2127.
(30) Platz, M. S.; Huang, H. Y.; Ford, F.; Toscano, J. Photochemical rearrangements of diazirines and thermal rearrangements of carbenes. *Pure Appl. Chem.* **1997**, *69*, 803−807.
(31) Motschiedler, K.; Gudmundsdottir, A.; Toscano, J. P.; Platz, M.; Garcia-Garibay, M. A. Excited Precursor Reactivity, Fast 1,2-H Shifts, and Diffusion-Controlled Methanol Insertion in 1,2-Diphenylalkylidenes. *J. Org. Chem.* **1999**, *64*, 5139−5147.
(32) Demchenko, A. P.; Tomin, V. I.; Chou, P. T. Breaking the Kasha Rule for More Efficient Photochemistry. *Chem. Rev.* **2017**, *117*, 13353−13381.
(33) Wang, Y.; Sitzmann, E. V.; Novak, F.; Dupuy, C.; Eisenthal, K. B. Reactions of Excited Triplet Diphenylcarbene Studied with Picosecond Lasers. *J. Am. Chem. Soc.* **1982**, *104*, 3238−3239.
(34) Casal, H. L.; Sugamori, S. E.; Scaiano, J. C. Study of Carbonyl Oxide Formation in the Reaction of Singlet Oxygen with Diphenyldiazomethane. *J. Am. Chem. Soc.* **1984**, *106*, 7623−7624.
(35) Sitzmann, E. V.; Langan, J. G.; Eisenthal, K. B. Picosecond Laser Studies of The Effects of Reactants on Intramolecular Energy Relaxation of Diphenykarbene: Reaction of Diphenylcarbene with Alcohols. *Chem. Phys. Lett.* **1984**, *112*, 111−116.
(36) Eisenthal, K. B.; Turro, N. J.; Sitzmann, E. V.; Gould, I. R.; Hefferon, G.; Langan, J.; Cha, Y. Singlet-Triplet Interconversion of Diphenylmethylene. Energetics, Dynamics and Reactivities of Different Spin States. *Tetrahedron* **1985**, *41*, 1543−1554.
(37) Griller, D.; Majewski, M.; McGimpsey, W. G.; Nazran, A. S.; Scaiano, J. C. Reaction of Diphenylcarbene with Diphenyldiazomethane. *J. Org. Chem.* **1988**, *53*, 1550−1553.
(38) Kirmse, W.; Kilian, J.; Steenken, S. Carbenes and the 0-H Bond: Spectroscopic Evidence for Protonation of Diarylcarbenes to Give Diarylcarbenium Ions. *J. Am. Chem. Soc.* **1990**, *112*, 6399−6400.
(39) Portella-Oberli, M. T.; Jeannin, C.; Soep, B.; Zerza, G.; Chergui, M. Femtosecond study of the rise and decay of carbenes in solution. *Chem. Phys. Lett.* **1998**, *296*, 323−328.
(40) Peon, J.; Polshakov, D.; Kohler, B. Solvent Reorganization Controls the Rate of Proton Transfer from Neat Alcohol Solvents to Singlet Diphenylcarbene. *J. Am. Chem. Soc.* **2002**, *124*, 6428−6438.
(41) Costa, P.; Sander, W. Hydrogen Bonding Switches the Spin State of Diphenylcarbene from Triplet to Singlet. *Angew. Chem., Int. Ed.* **2014**, *53*, 5122−5125.
(42) Costa, P.; Fernandez-Oliva, M.; Sanchez-Garcia, E.; Sander, W. The Highly Reactive Benzhydryl Cation Isolated and Stabilized in Water Ice. *J. Am. Chem. Soc.* **2014**, *136*, 15625−15630.
(43) Knorr, J.; Sokkar, P.; Schott, S.; Costa, P.; Thiel, W.; Sander, W.; Sanchez-Garcia, E.; Nuernberger, P. Competitive solvent-molecule interactions govern primary processes of diphenylcarbene in solvent mixtures. *Nature Commun.* **2016**, *7*, 12968.
(44) Knorr, J.; Sokkar, P.; Costa, P.; Sander, W.; Sanchez-Garcia, E.; Nuernberger, P. How Protic Solvents Determine the Reaction Mechanisms of Diphenylcarbene in Solution. *J. Org. Chem.* **2019**, *84*, 11450−11457.
(45) Ohno, M.; Itoh, M.; Umeda, M.; Furuta, R.; Kondo, K.; Eguchi, S. Conjugatively Stabilized Bridgehead Olefins: Formation and Reaction of Remarkably Stable Homoadamant-3-enes Substituted with Phenyl and Methoxycarbonyl Groups. *J. Am. Chem. Soc.* **1996**, *118*, 7075−7082.
(46) Fernández, I.; Frenking, G. Direct Estimate of the Strength of Conjugation and Hyperconjugation by the Energy Decomposition Analysis Method. *Chem. Eur. J.* **2006**, *12*, 3617−3629.
(47) Šumanovac, T.; Alešković, M.; Šekutor, M.; Matković, M.; Baron, T.; Mlinarić-Majerski, K.; Bohne, C.; Basarić, N. Photoelimination of Nitrogen from Diazirines: Spectroscopic Study and Supramolecular Control. *Photochem. Photobiol. Sci.* **2019**, *18*, 1806−1822.
(48) Hatchard, C. G.; Parker, C. A. A new sensitive chemical actinometer − II. Potassium ferrioxalate as a standard chemical actinometer. *Proc. R. Soc. Lond. A* **1956**, *235*, 518−536.
(49) Kuhn, H. J.; Braslavsky, S. E.; Schmidt, R. Chemical Actinometry. *Pure Appl. Chem.* **2004**, *76*, 2105−2146.
(50) Gerbig, D.; Ley, D. Computational Methods for Contemporary Carbene Chemistry. *WIREs Comput. Mol. Sci.* **2013**, *3*, 242−272.
(51) Snellenburg, J. J.; Laptenok, S. P.; Seger, R.; Mullen, K. M.; van Stokkum, I. H. M. *Glotaran*: A *Java*-Based Graphical User Interface for the *R* Package *TIMP*. *J. Stat. Sotfw.* **2012**, *49*, 1−22.
(52) Hirai, K.; Tomioka, H.; Okazaki, T.; Tokunaga, K.; Kitagawa, T.; Takeuchi, K. Laser Flash Photolysis of 3-noradamantyl(phenyl)-diazomethane: Generation, Detection and Kinetics of 2-phenyladamantene. *J. Phys. Org. Chem.* **1999**, *12*, 165−169.
(53) Tae, E. L.; Zhu, Z.; Platz, M. S. A Matrix Isolation, Laser Flash Photolysis, and Computational Study of Adamantene. *J. Phys. Chem. A* **2001**, *105*, 3803−3807.
(54) Montalti, M.; Credi, A.; Prodi, L.; Gandolfi, M. T. *Handbook of Photochemistry*, 3rd ed.; CRC Press: Boca Raton, FL, 2006.
(55) Nikšić-Franjić, I.; Ljubić, I. Comparing the Performances of Various Density Functionals for Modelling the Mechanisms and Kinetics of Bimolecular Free Radical reactions in Aqueous Solution. *Phys. Chem. Chem. Phys.* **2019**, *21*, 23425−23440.
(56) de Souza, B.; Farias, G.; Neese, F.; Izsak, R. Predicting Phosphorescence Rates of Light Organic Molecules Using Time-Dependent Density Functional Theory and the Path Integral Approach to Dynamics. *J. Chem. Theory Comput.* **2019**, *15*, 1896−1906.
(57) Forjan, M.; Zgrablić, G.; Vdović, S.; Šekutor, M.; Basarić, N.; Kabacinski, P.; Nazari Haghighi Pashaki, M.; Frey, H.-M.; Cannizzo, A.; Cerullo, G. Photogeneration of Quinone Methide from Adamantylphenol in an Ultrafast Non-adiabatic Dehydration Reaction. *Phys. Chem. Chem. Phys.* **2022**, *24*, 4384−4393.
(58) Liao, Y.; Bohne, C. Alcohol Effect on Equilibrium Constants and Dissociation Dynamics of Xanthone-Cyclodextrin Complexes. *J. Phys. Chem.* **1996**, *100*, 734−743.
(59) Pace, T. C. S.; Bohne, C. Temperature Effects on Xanthone-*β*-Cyclodextrin Binding Dynamics. *Can. J. Chem.* **2011**, *89*, 395−401.
(60) Yanai, T.; Tew, D. P.; Handy, N. C. A New Hybrid Exchange−Correlation Functional Using the Coulomb-Attenuating Method (CAM-B3LYP). *Chem. Phys. Lett.* **2004**, *393*, 51−57.
(61) Loos, P.-F.; Comin, M.; Blase, X.; Jacquemin, D. Reference Energies for Intramolecular Charge-Transfer Excitations. *J. Chem. Theory Comput.* **2021**, *17*, 3666−3686.
(62) Weigend, F.; Ahlrichs, R. Balanced Basis Sets of Split Valence, Triple Zeta Valence and Quadruple Zeta Valence Quality for H to Rn: Design and Assessment of Accuracy. *Phys. Chem. Chem. Phys.* **2005**, *7*, 3297−3305.
(63) Zheng, J.; Xu, X.; Truhlar, D. G. Minimally Augmented Karlsruhe Basis Sets. *Theor. Chem. Acc.* **2011**, *128*, 295−305.
(64) Neese, F.; Wennmohs, F.; Hansen, A.; Becker, U. Efficient, Approximate and Parallel Hartree−Fock and Hybrid DFT Calcu-

https://doi.org/10.1021/acs.joc.2c02875
J. Org. Chem. 2023, 88, 4286−4300

lations. A 'Chain-of-Spheres' Algorithm for the Hartree−Fock Exchange. *Chem. Phys.* **2009**, *356*, 98−109.
(65) Weigend, F. Accurate Coulomb-Fitting Basis Sets for H to Rn. *Phys. Chem. Chem. Phys.* **2006**, *8*, 1057−1065.
(66) Neese, F. An Improvement of the Resolution of the Identity Approximation for the Formation of the Coulomb Matrix. *J. Comput. Chem.* **2003**, *24*, 1740−1747.
(67) Mennucci, B. Polarizable Continuum Model. *WIREs Comput. Mol. Sci.* **2012**, *2*, 386−404.
(68) Barone, V.; Cossi, M. Quantum Calculation of Molecular Energies and Energy Gradients in Solution by a Conductor Solvent Model. *J. Phys. Chem. A* **1998**, *102*, 1995−2001.
(69) Scalmani, G.; Frisch, M. J. Continuous Surface Charge Polarizable Continuum Models of Solvation. I. General formalism. *J. Chem. Phys.* **2010**, *132*, 114110.
(70) Grimme, S.; Ehrlich, S.; Goerigk, L. Effect of the Damping Function in Dispersion Corrected Density Functional Theory. *J. Comput. Chem.* **2011**, *32*, 1456−65.
(71) Hirata, S.; Head-Gordon, M. Time-Dependent Density Functional theory within the Tamm−Dancoff Approximation. *Chem. Phys. Lett.* **1999**, *314*, 291−299.
(72) Martin, R. L. Natural Transition Orbitals. *J. Chem. Phys.* **2003**, *118*, 4775−4777.
(73) Ortiz, J. V. An Efficient, Renormalized Self-Energy for Calculating the Electron Binding Energies of Closed-Shell Molecules and Anions. *Int. J. Quantum Chem.* **2005**, *105*, 803−808.
(74) Dunning, T. H., Jr. Gaussian Basis Sets for Use in Correlated Molecular Calculations. I. The Atoms Boron through Neon and Hydrogen. *J. Chem. Phys.* **1989**, *90*, 1007−1023.
(75) Andersson, K.; Malmqvist, P.-Å.; Roos, B. O. Second-Order Perturbation Theory with a Complete Active Space Self-Consistent Field Reference Function. *J. Chem. Phys.* **1992**, *96*, 1218−1226.
(76) Forsberg, N.; Malmqvist, P.-Å. Multiconfiguration Perturbation Theory with Imaginary Level Shift. *Chem. Phys. Lett.* **1997**, *274*, 196−204.
(77) Ljubić, I.; Sabljić, A. CASSCF/CASPT2 and TD-DFT Study of Valence and Rydberg Electronic Transitions in Fluorene, Carbazole, Dibenzofuran, and Dibenzothiophene. *J. Phys. Chem. A* **2011**, *115*, 4840−4850.
(78) Ljubić, I.; Sabljić, A. Theoretical Study of Structure, Vibrational Frequencies, and Electronic Spectra of Polychlorinated Dibenzo-*p*-dioxins. *J. Phys. Chem. A* **2006**, *110*, 4524−4534.
(79) Malmqvist, P.-Å.; Roos, B. O. The CASSCF State Interaction Method. *Chem. Phys. Lett.* **1989**, *155*, 189−194.
(80) Frisch, M. J.; Trucks, G. W.; Schlegel, H. B.; Scuseria, G. E.; Robb, M. A.; Cheeseman, J. R.; Scalmani, G.; Barone, V.; Petersson, G. A.; Nakatsuji, H.; Li, X.; Caricato, M.; Marenich, A. V.; Bloino, J.; Janesko, B. G.; Gomperts, R.; Mennucci, B.; Hratchian, H. P.; Ortiz, J. V.; Izmaylov, A. F.; Sonnenberg, J. L.; Williams-Young, D.; Ding, F.; Lipparini, F.; Egidi, F.; Goings, J.; Peng, B.; Petrone, A.; Henderson, T.; Ranasinghe, D.; Zakrzewski, V. G.; Gao, J.; Rega, N.; Zheng, G.; Liang, W.; Hada, M.; Ehara, M.; Toyota, K.; Fukuda, R.; Hasegawa, J.; Ishida, M.; Nakajima, T.; Honda, Y.; Kitao, O.; Nakai, H.; Vreven, T.; Throssell, K.; Montgomery, Jr., J. A.; Peralta, J. E.; Ogliaro, F.; Bearpark, M. J.; Heyd, J. J.; Brothers, E. N.; Kudin, K. N.; Staroverov, V. N.; Keith, T. A.; Kobayashi, R.; Normand, J.; Raghavachari, K.; Rendell, A. P.; Burant, J. C.; Iyengar, S. S.; Tomasi, J.; Cossi, M.; Millam, J. M.; Klene, M.; Adamo, C.; Cammi, R.; Ochterski, J. W.; Martin, R. L.; Morokuma, K.; Farkas, O.; Foresman, J. B.; Fox, D. J. *Gaussian 16*, rev. C.01; Gaussian, Inc.: Wallingford, CT, 2016.
(81) Fdez. Galván, I.; Vacher, M.; Alavi, A.; Angeli, C.; Aquilante, F.; Autschbach, J.; Bao, J. J.; Bokarev, S. I.; Bogdanov, N. A.; Carlson, R. K.; Chibotaru, L. F.; Creutzberg, J.; Dattani, N.; Delcey, M. G.; Dong, S. S.; Dreuw, A.; Freitag, L.; Frutos, L. M.; Gagliardi, L.; Gendron, F.; Giussani, A.; González, L.; Grell, G.; Guo, M.; Hoyer, C. E.; Johansson, M.; Keller, S.; Knecht, S.; Kovačević, G.; Källman, E.; Manni, G. L.; Lundberg, M.; Ma, Y.; Mai, S.; Malhado, J. P.; Malmqvist, P. A.; Marquetand, P.; Mewes, S. A.; Norell, J.; Olivucci, M.; Oppel, M.; Phung, Q. M.; Pierloot, K.; Plasser, F.; Reiher, M.; Sand, A. M.; Schapiro, I.; Sharma, P.; Stein, C. J.; Sørensen, L. K.; Truhlar, D. G.; Ugandi, M.; Ungur, L.; Valentini, A.; Vancoillie, S.; Veryazov, V.; Weser, O.; Wesołowski, T. A.; Widmark, P.-O.; Wouters, S.; Zech, A.; Zobel, J. P.; Lindh, R. OpenMolcas: From Source Code to Insight. *J. Chem. Theory Comput.* **2019**, *15*, 5925−5964.
(82) Neese, F. The ORCA Program System. *WIREs Comput. Mol. Sci.* **2012**, *2*, 73−78.
(83) Neese, F. Software Update: The ORCA Program System, Version 4.0. *WIREs Comput. Mol. Sci.* **2018**, *8*, No. e1327.
(84) Dennington, R.; Keith, T. A.; Millam, J. M. *GaussView*, ver. 5; Semichem Inc: Shawnee Mission, KS, 2009.

https://doi.org/10.1021/acs.joc.2c02875
J. Org. Chem. 2023, 88, 4286−4300